THE ROLE OF LEAF AREA WITHIN PLANT CO_2 PHYSIOLOGICAL RESPONSES AND THE IMPACTS ON HYDROCLIMATE CHANGES

by

ALANA CORDAK

(Under the Direction of Gabriel Kooperman)

ABSTRACT

Atmospheric CO_2 concentrations have risen to almost 1.5x preindustrial values and could increase to nearly 3.9x preindustrial values by the end of the century, leading to innumerable effects on the climate. These impacts are largely associated with the enhanced greenhouse effect, but recent work also highlights plant physiological responses that can strongly influence water cycling. This study explores these plant responses to 2x preindustrial CO_2 concentrations by analyzing simulations from the Community Earth System Model versions 1 and 2. We find that leaf area plays an important role in hydrological cycle changes (e.g., precipitation, evapotranspiration, and runoff) through its influence on canopy evaporation, which can offset transpiration decreases from reduced stomatal conductance. Compared to the Advanced Very High Resolution Radiometer-derived leaf area, CESM2 better captures near present-day magnitudes but potentially overestimates leaf area-CO_2 sensitivity, highlighting the need to reduce plant-related biases for future climate research.

INDEX WORDS: Earth System Model, Hydrological Cycle, Plant Physiology

THE ROLE OF LEAF AREA WITHIN PLANT CO_2 PHYSIOLOGICAL RESPONSES AND THE IMPACTS ON HYDROCLIMATE CHANGES

by

ALANA CORDAK

BS, The University of Georgia, 2020

A Thesis Submitted to the Graduate Faculty of The University of Georgia in Partial Fulfillment of the Requirements for the Degree

MASTER OF SCIENCE

ATHENS, GEORGIA

2023

THE ROLE OF LEAF AREA WITHIN PLANT CO_2 PHYSIOLOGICAL RESPONSES AND THE IMPACTS ON HYDROCLIMATE CHANGES

by

ALANA CORDAK

Major Professor: Gabriel Kooperman
Committee: Abigail Swann
Thomas Mote

Electronic Version Approved:

Ron Walcott
Vice Provost for Graduate Education and Dean of the Graduate School
The University of Georgia
December 2023

DEDICATION

To my mom, who has always given me the love, support, and strength to weather all of life's storms (and climates).

ACKNOWLEDGEMENTS

We thank Claire Zarakas for sharing her controlled leaf area simulations and Tree2H2O for feedback and suggestions. This work is supported by the U.S. Department of Energy (DOE) Regional and Global Model Analysis Program (DE-SC0019459 and DE-SC0021209). The Community Earth System Model (CESM) development is led by the National Center for Atmospheric Research (NCAR) and supported by the National Science Foundation (NSF) and DOE. Computing and data storage resources, including the Cheyenne supercomputer (doi:10.5065/D6RX99HX), were provided by the Computational and Information Systems Laboratory (CISL) at NCAR.

TABLE OF CONTENTS

Page

LIST OF FIGURES

Page

CHAPTER 1

INTRODUCTION

Climate model projections from the Coupled Model Intercomparison Project Phase 6 (CMIP6) (Eyring et al., 2016), which provides results for the Intergovernmental Panel on Climate Change Sixth Assessment Report, include significant increases in atmospheric CO_2 concentrations by the end of the 21st century. The level of increase largely depends on future anthropogenic emissions and socioeconomic developments but reach as high as 800 and 1100 parts per million (ppm) by 2100 in scenarios with medium-high and high reliance on fossil fuels, respectively. With the continuous rise in CO_2, all parts of the earth climate system will be affected, including the hydrologic cycle. Changes to this cycle impact water resources and influence climate extremes, which have consequences for human societies and life on earth (e.g., drought and access to drinking water, floods and impacts on infrastructure and habitats, agriculture and food production) (Lee et al., 2021).

For example, with higher levels of global warming, global mean precipitation is expected to increase over the high latitudes, tropics, and large parts of the monsoon regions but decrease over the mid-latitudes and subtropics. These regional differences are projected to follow a "wet gets wetter, dry gets drier" pattern with some regions that are already dry and warm, such as southern Africa and the Mediterranean, expected to become progressively drier and warmer as global temperatures rise. However, this patten does not hold well over land because there are limits on moisture availability (Lee et al., 2021). Evaporation is also expected to increase but

with regional variations under future surface warming and differences in land water availability. Additionally, global runoff, including the rates of change, is projected to increase with global warming but with large regional and seasonal variations (e.g., increase in the northern high latitudes and decrease in the Mediterranean region and southern Africa) as it is a highly non-linear process depending on soil moisture and temperature thresholds (Arias et al., 2021; Douville et al., 2021). Overall, continued global warming is projected to further intensify the global water cycle, including its variability and extreme wet and dry events.

CO_2 driven changes to the climate system include both radiative (i.e., the enhanced greenhouse effect) and plant physiological responses. While the effects of plant CO_2 physiology (here after referred to as plant physiology) are not as large in magnitude compared to the CO_2 radiative effects on the earth system, plant responses can act to reinforce or diminish the influence of radiative responses (Skinner et al., 2017). For example, plant-centric variables and metrics reduce estimates of drought stress and severity compared to atmospheric-centric variables and metrics (Swann et al., 2016). However, projections of future flooding that take plant physiology into account suggest that plants can increase flood risk in many regions (Fowler et al., 2019). In addition, plant physiological responses contribute to the spread across different climate model projections, highlighting the need for improved understanding and representation of plant characteristics and processes in order to reduce model uncertainties (Zarakas et al., 2020).

When exposed to elevated levels of CO_2, plants increase their rates of photosynthesis, which allows for greater and/or faster growth (Prentice et al., 2001). This can result in increased biomass (i.e., CO_2 fertilization) (Norby & Zak, 2011), but the relative growth in a particular component (e.g., leaf area vs stems) may depend on different factors (e.g., the type and age of

the plant (Jiang et al., 2020), or the climate model representation of carbon allocation (Wieder et al., 2019)). Increased leaf area is particularly relevant to land-atmosphere coupling because it provides more canopy from which precipitation can collect and evaporate, leading to an increase in water loss through canopy evaporation (here after referred to as the leaf area response) (Hong et al., 2019). Additionally, plants reduce the opening of their stomata—pores on the leaves that control CO_2 uptake and water loss between the leaf interior and the atmosphere (Lawson & Vialet-Chabrand, 2019)—to optimize water use efficiency and carbon yield (Brodribb et al., 2020). This response, in contrast to leaf area, decreases water loss through transpiration (here after referred to as the stomatal conductance response) (Hong et al., 2019). These responses are not mutually exclusive from each other because changes in one component of total evaporation influence the evaporative demand experienced by the other components. Additionally, the stomatal conductance response is partially influenced by leaf area changes as increases in leaf area increase the number of stomata.

These vegetation-related processes influence the overall water fluxes between the land and atmosphere (Allan et al., 2020), and thus, the balance between the leaf area and stomatal conductance responses can greatly influence the hydroclimate. Existing literature has highlighted the important and potentially competing roles of both processes. For example, some studies find that the leaf area response outpaces other effects on hydrological changes (Frank et al., 2015; Guerrieri et al., 2019; Mankin et al., 2017; Mankin et al., 2018; Mankin et al., 2019; McDermid et al, 2021; Singh et al., 2020; Zhu et al., 2021), while others suggest that the stomatal conductance response more strongly influences the hydroclimate (Berg & McColl, 2021; Fowler et al., 2019; Hong et al., 2019; Jiang et al., 2021; Kooperman et al., 2018b; Lemordant et al., 2018; Lian et al., 2021; Skinner et al., 2017; Swann et al., 2016; Zarakas et al., 2020; Zhang et

al., 2021). These conflicting conclusions can result from assessments of different regions (e.g., comparing the mid-latitude to the tropics), variables (e.g., evapotranspiration versus soil moisture), or levels of CO_2 increase rather than differences in the physical understanding. They can also result from different models and/or parameterizations used, and thus, the dominant plant physiological response can vary across the studies. These results also highlight the ongoing uncertainty in the literature related to these plant interactions and the need for continued work to improve their representation in models.

This study aims to highlight the influence of plant-related processes in simulations of land-atmosphere interactions and climate change. In particular, we aim to better understand the complexities of how leaf area index (LAI) growth and its sensitivity to changes in CO_2 concentrations impact the global water cycle. Because there are many biases and uncertainties related to how plants are represented in Earth system models, often with coupled and/or competing influences on climate projections, we mainly focus on leaf area using simulations that allow us to better understand its influence on hydrological cycle changes.

CHAPTER 2

METHODS

Community Earth System Model

We analyze output from the National Center for Atmospheric Research's fully coupled and interactive Community Earth System Model (CESM) versions 1 and 2 (CESM1, Lindsay et al., 2014; CESM2, Danabasoglu et al., 2020). We focus primarily on the land component, which is the Community Land Model (CLM4, Oleson et al., 2010, Lawrence et al., 2011; CLM5, Lawrence et al., 2018, Lawrence et al., 2019). CLM represents a variety of plant types and processes and interacts with other components of CESM, including two-way coupling with the atmosphere component, the Community Atmosphere Model (CAM4, Neale et al., 2010; CAM6, UCAR 2017). CLM simulates many biogeophysical and biogeochemical processes for each subgrid land unit, column, and plant functional type. The processes of interest in this study are related to canopy and soil hydrology (e.g., canopy interception, throughfall, canopy drip, infiltration, evaporation, surface runoff), and stomatal physiology and photosynthesis. These processes are responsive to the overlying conditions simulated by CAM, such as precipitation, downwelling radiation, wind, temperature and humidity, and influence latent and sensible heat fluxes, upwelling shortwave and longwave radiation, and surface roughness, provided as the bottom boundary conditions for CAM.

CLM5 contains several updates to processes and parameterizations in CLM4, some of which help to improve the model's representation of the hydrologic cycle. One such update is to

the stomatal conductance model. The default stomatal conductance calculation changed from the Ball-Berry model (Ball et al., 1987; Oleson et al., 2010) used in CLM4 to the Medlyn conductance model (Medlyn et al., 2011) used in CLM5. The Ball-Berry conductance model relates stomatal conductance to the net photosynthesis rate, relative humidity, and the CO_2 concentration at the leaf surface. The Medlyn conductance model combines both empirical (i.e., the observed stomatal responses to environmental conditions) and optimal approaches (i.e., the minimization of water used per unit carbon gained) and has been shown to have more realistic behavior at low humidity levels (Rogers et al., 2017). In addition, the carbon allocation scheme changed from dynamic (i.e., carbon allocation to stems versus leaves depends on net primary production) to fixed (i.e., relative carbon allocation to stems versus leaves is constant) in the update from CLM4 to CLM5 (Wieder et al., 2019). The dynamic scheme was replaced by the fixed scheme because it overestimates gross primary production and above ground biomass (including leaf area) (Montané et al., 2017; Negrón-Juárez et al., 2015), but biomass accumulation and leaf area growth over time are larger in the fixed scheme (Montané et al., 2017; Wieder et al., 2019). This then has consequences for the two model versions, with more carbon potentially being allocated to leaves in CESM2. These representations of stomatal conductance and leaf growth can exert strong controls on the plant CO_2 physiological responses described above. It is also important to note that neither version of CLM includes internal dynamic vegetation (i.e., plants can change their leaf area and stomatal opening, but the fraction of plant functional types is fixed within each grid cell), which has consequences for plant physiology and climate changes.

In the analysis below, we intercompare two sets of controlled simulations. The first compares simulations with and without leaf area changes within a single model (CESM2). The

second compares simulations from CESM1 and CESM2 with the differences in parameterizations described above. Previous studies have shown that plant physiological effects greatly contribute to hydrological cycle changes in the Coupled Model Intercomparison Project Phase 5 (CMIP5) models (Taylor et al., 2012) (Kooperman et al., 2018a;b; Swann et al., 2016), particularly in CESM1. For example, in simulations with rising CO_2, most CMIP5 models show that plant effects have larger contributions to evaporation and precipitation minus evaporation changes compared to radiative effects (Figure 1). However, recent work with CMIP6 models, including CESM2, shows smaller plant effects on hydrological changes under elevated CO_2. For example, Cornish et al. (2023, in-prep) found that global-land mean evapotranspiration changes by -0.1788 mm/day in CESM1 but only by -0.0823 mm/day in CESM2, with a range of changes between -0.0419 mm/day and -0.2063 mm/day across the CMIP6 models. The reasons for this difference and the contribution of leaf area changes are explored using the simulations described below.

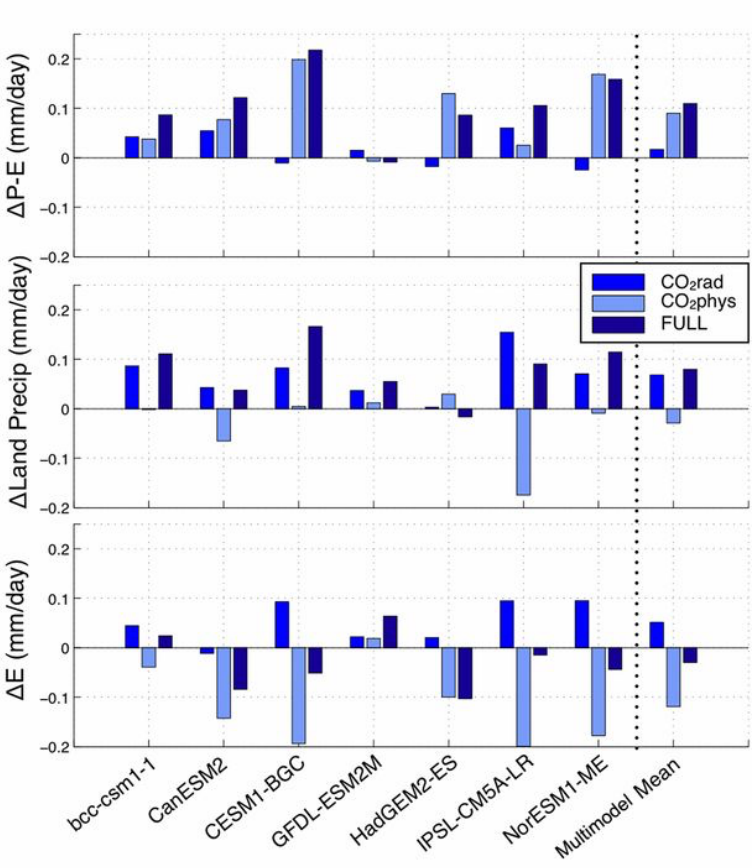

Figure 1. Average mid-latitude and low-latitude hydrologic cycle changes over land and the attribution to plant physiological and radiative effects of CO_2 (*from Swann et al., 2016*).

Coupled Climate Carbon Cycle Model Intercomparison Project (CESM1 & CESM2)

The Coupled Climate Carbon Cycle Model Intercomparison Project (C4MIP) experiments are designed to separate the plant physiological and radiative contributions to CO_2-driven changes and quantify the feedbacks between the carbon cycle and climate (Jones et al., 2016). These experiments are idealized, carbon concentration-driven scenarios, each ran for 140 simulation years, in which CO_2 increases by 1% per year from preindustrial levels (285ppm) to a quadrupling of these levels (1140ppm). In the first experiment, CO_2 increases affect both the atmosphere (radiative) and surface (plant) conditions (referred to as the full experiment). In

another experiment, only the surface experiences the increasing CO_2 levels while the atmosphere experiences constant preindustrial CO_2 levels, and this allows us to parse out the plant physiological contributions (here after referred to as the phys-only experiment**)**. In contrast, in a third simulation, only the atmosphere experiences the increasing CO_2 levels while the surface experiences constant preindustrial CO_2 levels in order to focus on the radiative contributions (referred to as rad-only experiment). In all these simulations, only the CO_2 concentration changes while preindustrial land cover and land use are used. In the phys-only experiment, changes in temperature and climate are only driven by land-surface responses, so it represents a cooler world because there is no enhanced radiative greenhouse effect as there is in the rad-only and full experiments. For the analysis here, the first 20 years of these simulations are used as preindustrial conditions, years 60 to 80 are 2x preindustrial CO_2 (i.e., CO_2 doubles at year 70), and the last 20 years are 4x preindustrial CO_2.

Historical and ScenarioMIP Simulations (CESM1 & CESM2)

For comparison, we also assess changes in the historical and scenario simulations. The historical simulation of the recent past (i.e., 1850 to 2005 and 1850 to 2014 for CMIP5 and CMIP6, respectively) imposes changing conditions (e.g., land cover and land use changes, changes in greenhouse gas concentrations and aerosols emissions) that are consistent with observations. The simulation is often used to evaluate model performance against present climate and observed climate changes (Eyring et al., 2016). The Scenario Model Intercomparison Project (ScenarioMIP) (O'Neill et al., 2016) provides near and long-term climate projections based on CMIP5 Representative Concentration Pathways (RCPs) (2006 to 2100) and CMIP6 Shared Socioeconomic Pathways (SSPs) (2015 to 2100), which are scenarios of future developments of

anthropogenic drivers of climate change, such as greenhouse gas and aerosol emissions, land use changes, and socioeconomic developments (van Vuuren et al., 2011). In the scenarios that include strong reliance on fossil fuels, the strongest driving factor is the forcing from CO_2. As a result, most of the hydrological cycle changes in the RCP8.5 and SSP5-8.5 scenarios (i.e., high emissions scenarios) are captured in the C4MIP experiments (e.g., Fowler et al., 2019; Kooperman et al., 2018a). These high emissions scenarios also magnify the signal of plant responses given their high CO_2 growth rate, thereby facilitating process understanding (Zhang 2022).

Fixed and Dynamic Leaf Area Simulations (CESM2)

Two sets of simulations using CESM2 with fixed and dynamic leaf area provide a controlled sensitivity experiment within a single model framework. In one set of simulations, leaf area index (LAI) is held constant or fixed (here after referred to as the fixed run) at annually repeating preindustrial values (i.e., no responses to changes in CO_2 or interannual variability). In another set of simulations, LAI is able to change dynamically with changes in CO_2 and the climate (here after referred to as the dynamic run). For each set, two simulations were run—one with CO_2 concentrations at preindustrial levels (285ppm) and another with an abrupt increase to 2x preindustrial levels (570ppm). The 2x preindustrial CO_2 simulations branched from the preindustrial CO_2 runs. Similar to the C4MIP phys-only experiments, these runs help isolate the plant physiological contributions to CO_2-driven changes in which only the land surface experiences the abrupt 2x preindustrial CO_2 levels while the atmosphere experiences constant preindustrial CO_2 levels. These simulations were run for 160 years, and in our analysis of the 2x preindustrial CO_2 conditions, we assess averages for 120 years, excluding the first 30 to 40 years.

This allows time for the plants to adjust to the abrupt CO_2 change because LAI can take several decades to reach a new equilibrium state. Additionally, the large averaging time helps capture the CO_2 signal amid large amounts of natural variability. Both of the fixed runs prescribe the LAI and stem area index (called satellite phenology mode in CESM), which are taken from the dynamic preindustrial run and adjusted such that interpolating between monthly midpoints gives the same monthly average as the dynamic run with preindustrial CO_2 (Neely et al., 2014).

Observations

In order to understand how the representation of simulated LAI values influences the results, we compare the various CESM simulations to observations. In this analysis, we evaluate the baseline LAI values and their sensitivities from CESM to LAI derived from the National Oceanic and Atmospheric Administration Climate Data Record of Advanced Very High Resolution Radiometer (AVHRR) Surface Reflectance, aggregated to monthly averages and corrected for unrealistic values (Claverie et al., 2016; Vermote, 2019). We then averaged the data for the years 1991 to 2010, excluded areas with a minimal amount of plants (i.e., non-vegetated areas), and re-gridded the data to the CESM grid. AVHRR provides estimates of global cloud cover, sea surface temperature, ice, snow and vegetation cover characteristics twice a day at 1 km resolution in the visible and infrared bands (Holben, 1986). Additionally, both AVHRR and AVH15C1 are referenced, but both datasets were generated from AVHRR leaf area observations, only differing by original spatial resolutions (i.e., 0.05 and 0.0833 degree, respectively), temporal resolutions (i.e., monthly and daily, respectively), and time periods (i.e., 1981 to 2011 and 1981 to 2019, respectively).

As with all datasets, there are also biases and limitations associated with the LAI derived from the AVHRR Surface Reflectance. Compared to in situ data from BELMANIP2 (BEnchmark Land Multisite ANalysis and Intercomparison of Products 2) and DIRECT network sites, the derived LAI is consistent and reliable and performs well for cropland, grassland, and non-vegetated surfaces. However, the product is unable to reproduce the variability of densely vegetated cover, such as in deciduous or broadleaf forest biomes (e.g., a clear saturation effect occurs in these biomes with high LAI values) (Claverie et al., 2016). These limitations can make it difficult to assess simulated LAI biases, influencing the reliability of these observed LAI values across different global regions. Additionally, tropical regions tend to dominate the global LAI signal, adding additional complexity to LAI assessments.

We now explore the differences in the various simulations, the contribution of leaf area changes, and the differences in the simulated and observed LAI using the methods described above. The first section compares the changes in the hydrological cycle with varying leaf area changes using the fixed and dynamic leaf area simulations and the C4MIP experiments. The second section focuses on the changes in leaf area and the components of the hydrological cycle in order to assess the processes that drive leaf area impacts on total evaporation. The last section compares simulated leaf area and its sensitivity to changes in CO_2 to observations.

CHAPTER 3

RESULTS

Section 1: Hydrological Cycle Changes due to Plant CO_2 Physiological Effects

We begin by assessing the plant physiological effects on the hydrological cycle with and without leaf area changes in the controlled set of CESM2 simulations with dynamic and fixed leaf area, respectively. When comparing the changes from preindustrial CO_2 to a doubling of preindustrial CO_2, the fixed run generally exhibits a decrease in total evaporation across the global land masses, an increase in runoff everywhere except northeastern South America, and a zonally asymmetric pattern of precipitation change across tropical forests regions (i.e., a decrease over the Amazon and increases over Central Africa and the Maritime Continent) noted in previous work (Kooperman et al., 2018a,b) (Figure 2). Additionally, the fixed run precipitation pattern is similar to the total runoff pattern, with the exception of areas in China and Australia where runoff increases despite declines in precipitation. These similar patterns occur, in part, because increases in water input into the land via precipitation must be balanced by changes in evaporation, runoff, or storage in the long-term average (Lemordant et al., 2018). For instance, precipitation increases in central Africa, but total evaporation also decreases in this region, so the increased input of water contributes to larger runoff. However, changes in average precipitation do not exhibit one-to-one relationships with changes in average runoff because land-surface conditions and vegetation influence evaporation, and higher-level statistics of precipitation (e.g.,

precipitation type and intensity) can impact water infiltration into the soil beyond annual mean rates.

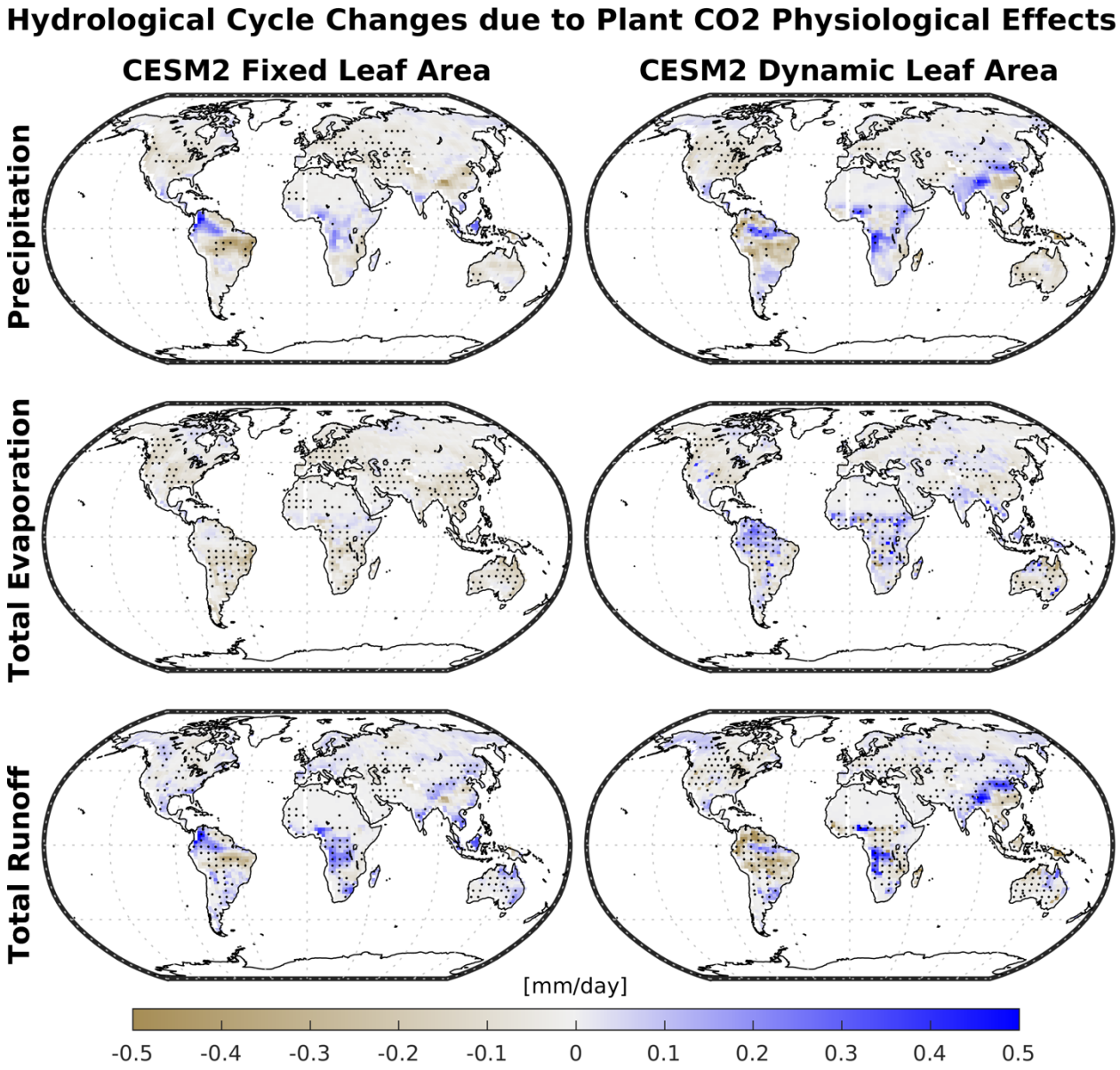

Figure 2. Changes in precipitation, total evaporation, and total runoff between preindustrial CO_2 and 2x preindustrial CO_2 for CESM2 fixed [left column] and dynamic [right column] leaf area phys-only runs. Stippling represents 90% significance, calculated using a paired t-test and an alpha value of 0.1.

The hydrologic changes in the dynamic run exhibit some differences from the fixed run, particularly across the tropics (Figure 2; preindustrial values in Figure S1). The changes in the dynamic run include an increase in evaporation over most land masses and a reversal of the total runoff increases seen in the fixed run over the tropical Andes, Central Africa, and the Maritime Continent. Runoff also increases more in parts of the Democratic Republic of the Congo, Angola, and northern China, including a small increase along the Amazon River. The pattern of precipitation change from preindustrial CO_2 to 2x preindustrial CO_2 in the dynamic run is more consistent with total runoff than it was in the fixed run and even reverses the fixed run pattern over northern South America (i.e., precipitation declines over the Andes and increases to the east). Precipitation also declines over the dense tropical forest regions in Central Africa and the Maritime Continent while it increases on the northern and southern boundaries of the Central African tropical forests and in India and northern China.

These changes are based on long climatological averages and are generally significant for total evaporation and runoff across the tropics. However, for both runs, precipitation has the least amount of area with significant changes compared to the other hydrological components, likely due to its larger interannual variability. Also, 2x preindustrial CO_2 is a smaller perturbation than has been used in most previous analyses of plant physiological effects, and thus, a strong signal may not emerge in many regions until CO_2 reaches a higher concentration. Nevertheless, even at 2x preindustrial CO_2, the plant effects on hydroclimate changes are evident. And because both the fixed and dynamic runs include the effects of stomatal conductance and only differ by the ability of leaf area to respond to CO_2 and climate changes, this indicates that both plant responses can significantly contribute to changes in the hydroclimate.

A follow-up question then is whether we can see the separate influences of these effects in results from the more commonly used C4MIP experiments, and whether the role of leaf area is also evident in those simulations. In particular, there is a large difference in leaf area growth between CESM1 and CESM2, which may relate to the ways that carbon is allocated in plants between the two model versions and ultimately contributes to differences in the plant physiological impacts on the climate. CESM2 C4MIP has a large increase in LAI at 2x preindustrial CO_2, similar to the dynamic run (Figure 3), which continues to increase through 4x preindustrial CO_2 (Figure S2). In contrast, CESM1 C4MIP has a smaller LAI increase at both elevated CO_2 levels. Next, we assess how these leaf area changes in the C4MIP experiments contribute to differences in the simulated hydroclimate changes.

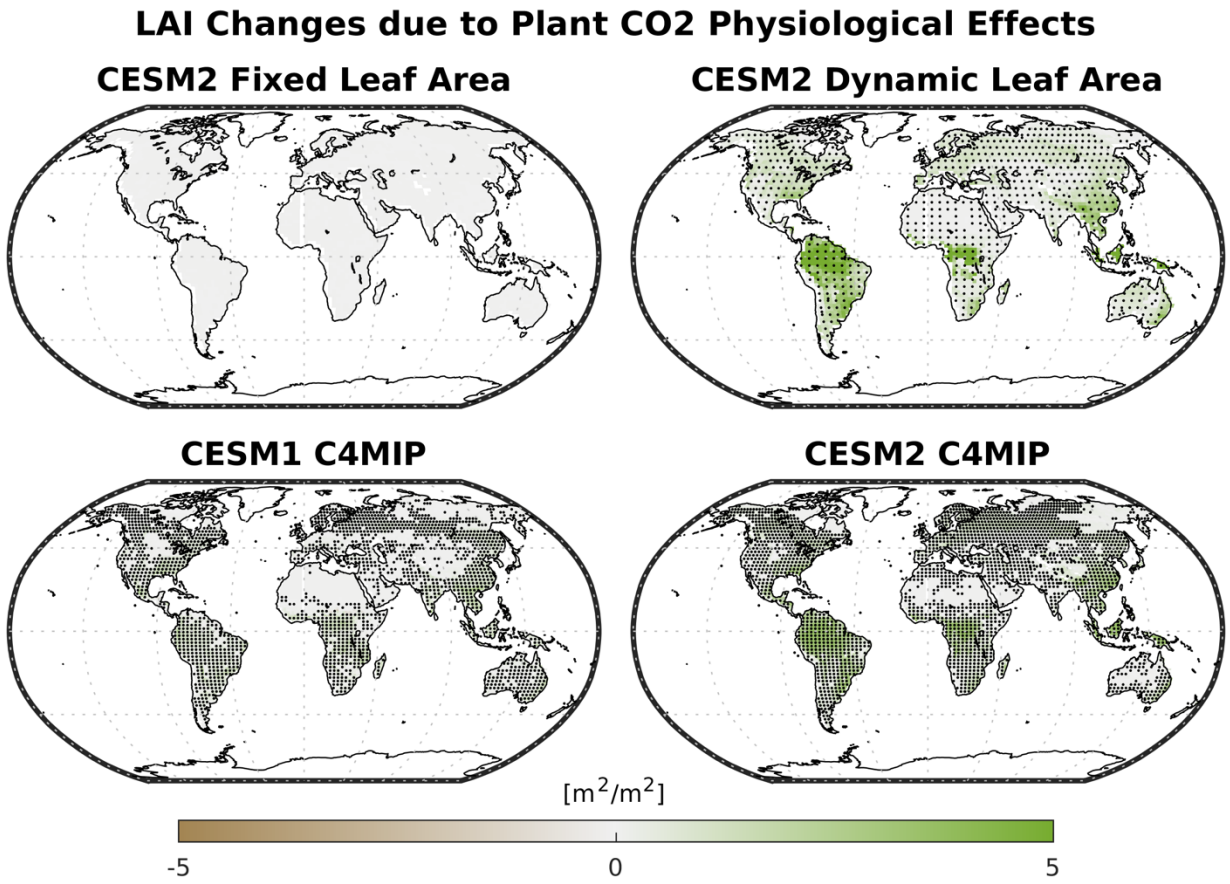

Figure 3. Changes in leaf area index between preindustrial CO_2 and 2x preindustrial CO_2 for CESM2 fixed and dynamic leaf area phys-only runs [top row] and CESM1 and CESM2 C4MIP phys-only experiments [bottom row]. Stippling represents 90% significance, calculated using a paired t-test and an alpha value of 0.1.

CESM1 and CESM2 have several different representations of important physical processes across all components of the model that can contribute to contrasting hydrological changes. Therefore, it can be more difficult to attribute differences due to leaf area or other changes related to CO_2 in comparison to the fixed and dynamic runs. However, there are some similarities between the C4MIP experiment differences and the fixed and dynamic run differences. For example, total evaporation in CESM1 C4MIP generally decreases across the

globe from preindustrial CO_2 to 2x preindustrial CO_2 (Figure 4; preindustrial values in Figure S3), which is consistent with changes in LAI and the fixed run. In contrast, CESM2 C4MIP total evaporation exhibits more spatial heterogeneity with both increases and decreases across the globe. While the magnitudes of change differ, these model differences in total evaporation changes are qualitatively consistent with the LAI effect on the differences between the CESM2 fixed and dynamic runs (Figure 2) (i.e., both CESM1 C4MIP and CESM2 fixed total evaporation generally decrease, while CESM2 C4MIP and CESM2 dynamic total evaporation have more areas that increase).

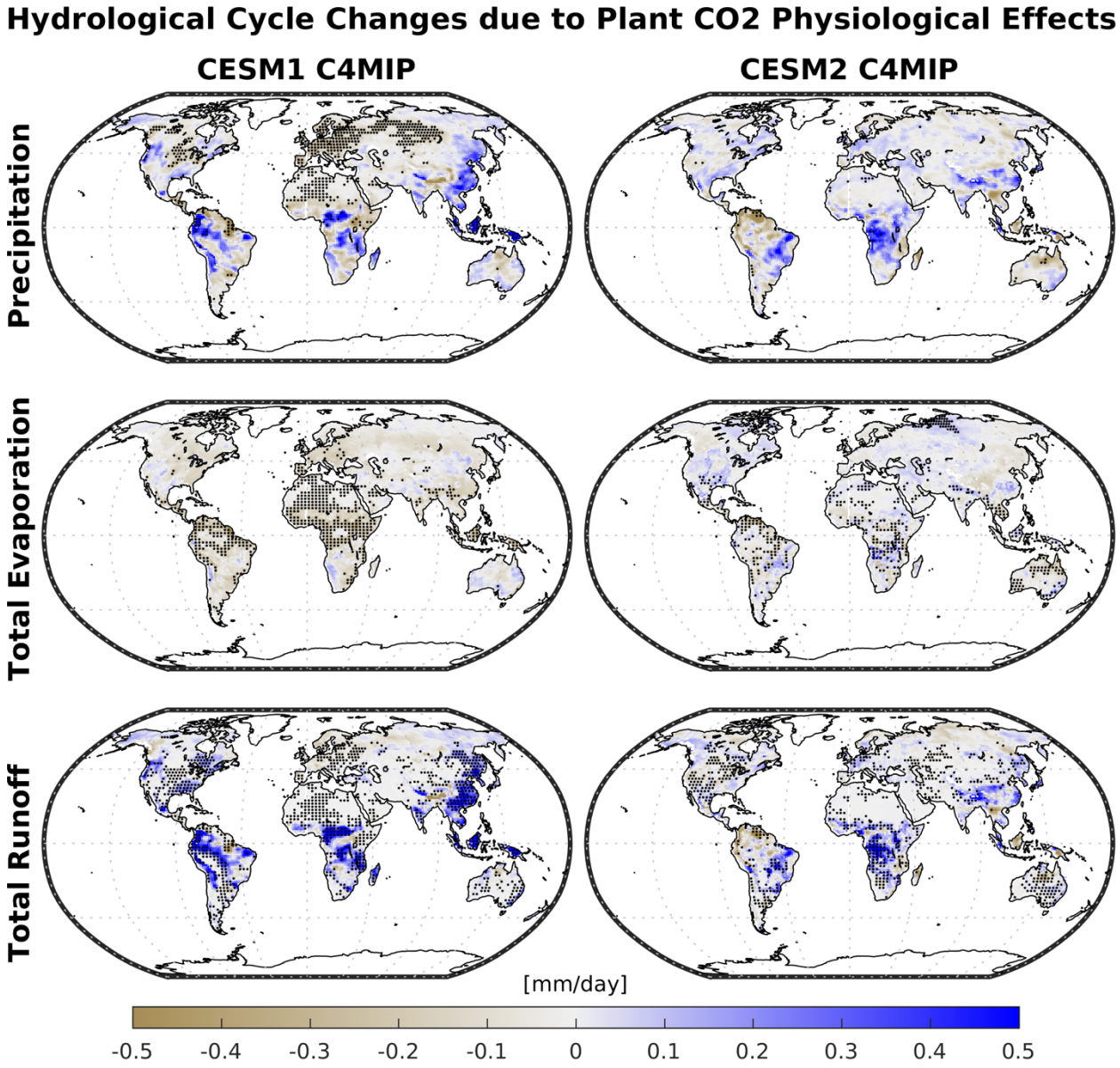

Figure 4. Changes in precipitation, total evaporation, and total runoff between preindustrial CO_2 and 2x preindustrial CO_2 for CESM1 [left column] and CESM2 [right column] C4MIP phys-only experiments. Stippling represents 90% significance, calculated using a paired t-test and an alpha value of 0.1.

In addition to the differences in total evaporation between the two C4MIP experiments, there are also different global patterns in precipitation and total runoff between the experiments. In CESM1, both precipitation and total runoff greatly increase on the coastal side of Asia, across the Maritime Continent, in parts of Central Africa, and along the western side of South America. These changes are consistent with what has been found previously in CESM1 C4MIP simulations at 4x preindustrial CO_2 in which the plant physiological effects were shown to contribute significantly to the full changes (i.e., both physiology and radiative effects) (Kooperman et al., 2018a;b; Swann et al., 2016). In CESM2, the magnitudes of these precipitation and runoff changes are slightly weaker or are even of opposite sign in these regions (e.g., the Andes and Maritime Continent regions decrease in precipitation and runoff but increase in CESM1). CESM2 total runoff also exhibits weaker increases compared to CESM1, which is related to the slight increase (or weaker decrease) in total evaporation, leaving comparatively less water in the soil column to contribute to runoff generation. Overall, the C4MIP precipitation patterns look similar to their respective total runoff patterns although there are places where the sign of the change flips (e.g., parts of Russia and the central United States in CESM1) and the relative magnitude varies.

Also similar to the fixed and dynamic runs, CESM2 C4MIP precipitation has the smallest amount of global area with significant changes between preindustrial CO_2 and 2x preindustrial CO_2 compared to the other hydrological components, with even less stippling than in the fixed and dynamic runs. A possible reason for this lack of significance could be that we only compare twenty-year periods, so the signal at 2x preindustrial CO_2, particularly for precipitation changes, may remain small compared to interannual variability, averages over longer time periods as in the fixed and dynamic runs, and changes at 4x preindustrial CO_2 (Figure S4). At 4x preindustrial

CO_2, a prominent difference is the consistent decrease in total evaporation over the majority of the global land masses in CESM2, which might suggest that stomatal closure becomes more important than LAI changes in CESM2 at higher CO_2 levels. But in general, these results suggests that the changes at 2x preindustrial CO_2 are representative of the direction and patterns of change under higher CO_2 conditions.

Overall, the global changes in these major hydrological components are not identical between the CESM2 fixed and dynamic runs and the CESM1 and CESM2 C4MIP experiments, but they share many meaningful similarities. And while the differences between the C4MIP experiments cannot be solely attributed to changes in leaf area as in the fixed and dynamic runs, these results demonstrate that leaf area likely plays an important role in changes to the hydroclimate, particularly in changes to total evaporation. In the next section, we explore the processes that drive the leaf area impacts on total evaporation.

Section 2: Changes in Leaf Area and Hydrological Cycle Components

When globally averaged, total evaporation decreases much more in response to higher CO_2 in the CESM2 fixed run than in the dynamic run (Figure 5; preindustrial values in Figure S5). Separating total evaporation into its individual components (i.e., canopy evaporation, transpiration, and soil evaporation) (spatial patterns in Figures S6 and S7) helps to clarify the specific mechanisms involving leaf area changes that lead to this difference. The increase in leaf area in response to elevated CO_2 in the dynamic run (yellow bar) provides more surface area from which rainwater can be collected and re-evaporated, leading to an increase in water loss through canopy evaporation. This increase in canopy evaporation then offsets the decrease in transpiration from stomatal conductance and reduces the overall change in total evaporation.

This decrease in transpiration is also slightly less in the dynamic run relative to the fixed run, likely due to the increase in the number of stomata with increased leaf area. Additionally, soil evaporation decreases slightly, but this is consistent with less precipitation reaching the surface due to greater leaf area coverage. Consequently, the balance between canopy evaporation and transpiration results in the seemingly smaller plant physiological impacts on the hydroclimate in the dynamic run. In contrast, leaf area in the fixed run does not change from preindustrial levels (i.e., missing red bar for LAI), so the change in canopy evaporation is smaller. With a smaller change in canopy evaporation, the decrease in transpiration is not offset, leaving transpiration as the largest contributor to the change in total evaporation in the fixed run. Additionally, because there is a slight decrease in global precipitation in the fixed run, it can be deduced that the small increases in canopy and soil evaporation are driven by higher evaporative demand on those components in response to the decline in transpiration.

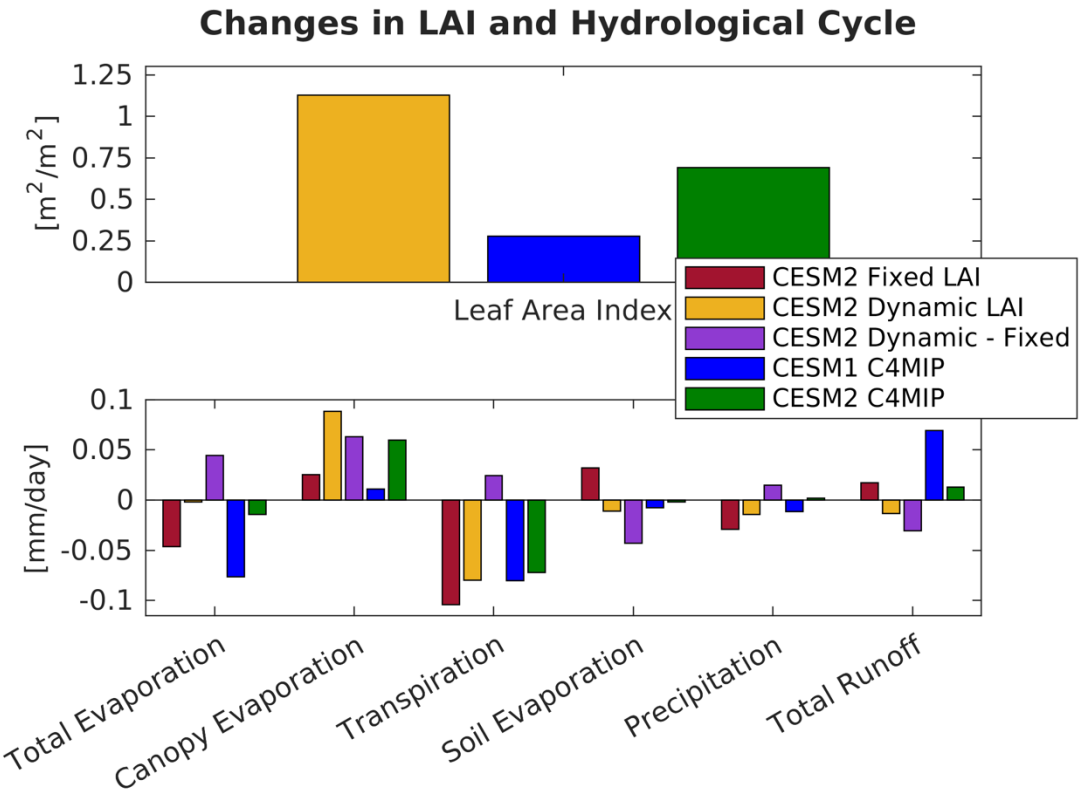

Figure 5. Global land averaged changes (excluding glacier regions) in leaf area index, total evaporation, components of total evaporation (i.e., canopy evaporation, transpiration, and soil evaporation), precipitation, and total runoff between preindustrial CO_2 and 2x preindustrial CO_2 for CESM2 fixed [red bars], dynamic [yellow bars], dynamic minus fixed [purple bars] phys-only leaf area runs, and CESM1 [blue bars] and CESM2 [green bars] C4MIP phys-only experiments.

As mentioned previously, while changes in leaf area cannot solely explain the differences between the CESM1 and CESM2 C4MIP experiments, the differences in total evaporation between the C4MIP experiments are similar to the differences between the CESM2 fixed and dynamic runs (Figure 5; spatial patterns compared previously in Figures 2 and 4). The larger increase in LAI in CESM2 C4MIP (green bar) compared to CESM1 C4MIP (blue bar) results in

a greater increase in canopy evaporation (spatial patterns in Figures S8, S9, and S10). Similar to the dynamic run, this increase then offsets the decrease in transpiration, resulting in a smaller change in total evaporation at higher CO_2 concentrations, and the seemingly smaller CESM2 plant physiological impacts on the overall hydroclimate. Additionally, greater leaf area changes in the dynamic leaf area and CESM2 C4MIP simulations lead to consistent changes in precipitation and runoff on global scales compared to their counterpart simulations with smaller leaf area changes.

While these simulations cannot completely isolate the leaf area response from the stomatal conductance response, they can still indirectly assess the added leaf area contribution (dynamic minus fixed run/purple bar) to the stomatal effect (fixed run/red bar) (Figure 5; spatial patterns in Figures S11 and S12). Focusing on this added contribution, leaf area exhibits a large increase in canopy evaporation (the largest contribution to its total evaporation change), a weak increase in transpiration (thereby decreasing the stomatal conductance response), and a decrease in soil evaporation. These changes then contribute to global mean increases in total evaporation (opposing the decrease from the stomatal effect) and precipitation, and a global mean decrease in total runoff.

Overall, these results demonstrate that plant physiological responses, including leaf area, are important for assessing changes to the hydrological cycle, and can naturally lead to an interest in how simulated leaf area and its sensitivity to changes in CO_2 compare to observations. This requires in-depth analysis and is often limited by the availability and quality of global-scale observations, but we briefly assess the differences in the next section.

Section 3: Leaf Area Biases in Baseline Values and CO_2 Sensitivity

LAI in the CESM2 fixed and dynamic leaf area runs (red and yellow bars) start at much higher values compared to the CESM2 C4MIP experiment (green bar) at preindustrial CO_2 (Figure S5; spatial patterns in Figure S13). For leaf area-CO_2 sensitivity, or the amount of leaf area change for a given change in CO_2, LAI increases more in the CESM2 dynamic and C4MIP simulations (yellow and green bars) than in the CESM1 C4MIP simulation (blue bar), with CESM2 dynamic LAI increasing the most (Figure 5; spatial patterns in Figure 3). These differences in the preindustrial values and CO_2 sensitivities are also evident in the relationship between global land average LAI and atmospheric CO_2 concentration (Figure 6). Because the C4MIP experiments do not include the radiative effects of CO_2, or other forcings such as changes in land use or aerosol emissions, they may not be directly comparable to near present-day observations. However, for LAI, they appear to capture the majority of the change found in the historical and scenario simulations, which include all forcings (similarity between the blue and green dotted and solid lines). This is consistent with previous literature (Kooperman et al., 2018a) which has shown that the C4MIP experiments capture much of the signal, even for tropical precipitation patterns, found in more realistic CMIP5 RCP8.5 simulations, implying that changes in CO_2 drive most of the projected changes in the climate.

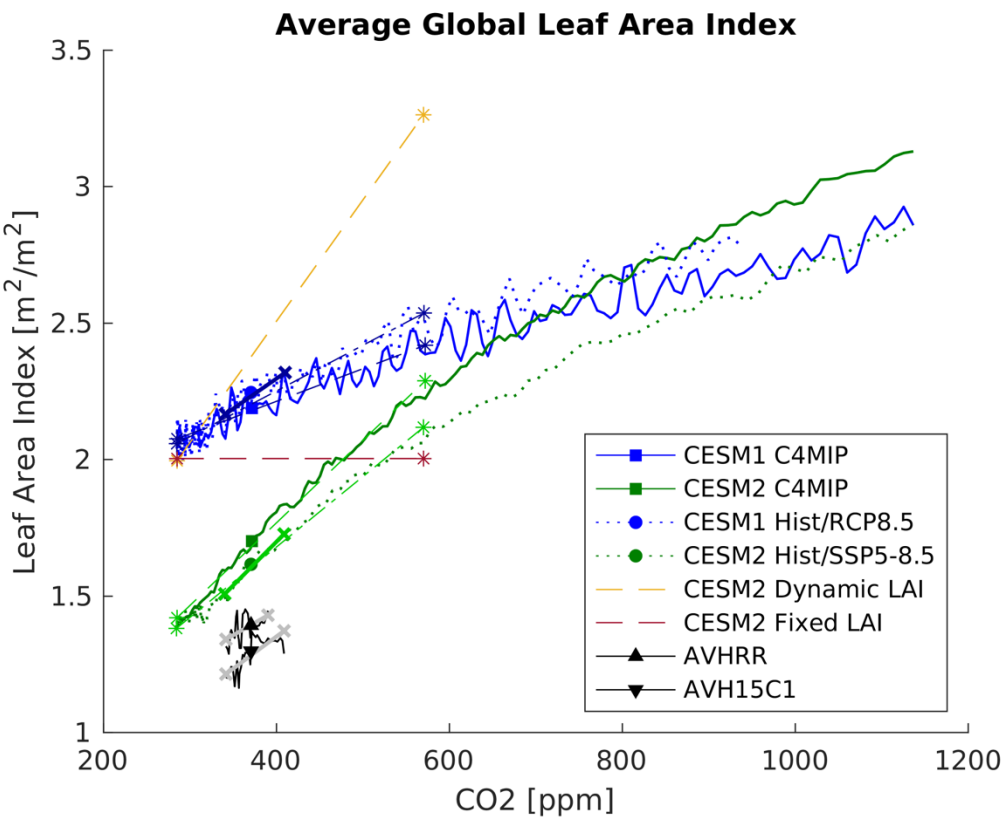

Figure 6. Leaf area as a function of CO_2 in CESM1 and CESM2 C4MIP phys-only [blue and green solid lines], CESM1 and CESM2 historical extended with RCP8.5/SSP5-8.5 [blue and green dotted lines], and CESM2 dynamic and fixed leaf area phys-only simulations [yellow and red dashed lines], and AVHRR and AVH15C1 observations [black solid lines]. Thicker solid lines with crosses represent leaf area-CO_2 sensitivities at near present-day CO_2 concentrations. Squares, circles, and triangles represent LAI values at near present-day CO_2 concentrations. Asterisks represent LAI values at preindustrial CO_2 and 2x preindustrial CO_2 concentrations.

We assess the LAI values averaged around present-day CO_2 concentrations (circles, squares, and triangles in Figure 6**;** spatial patterns in Figure S14), which show that CESM1 greatly overestimates global LAI compared to observations. CESM2 also overestimates observed leaf area but is closer to the observations, and this improvement is the result of reduced LAI

values over much of the globe, particularly in the tropics (Figures S15 and S16). One thing to note, however, is that AVHRR underestimates LAI in biomes with dense vegetation, such as in the tropics, so these biases could be less extreme with other observations that provide greater accuracy. Nevertheless, these overestimates in leaf area are consistent with a study by Song et al. (2020), which found that all of the CMIP6 models and the multi-model ensemble mean (MME) generally reproduce the observed LAI spatial pattern but overestimate the global mean (ranging from 1.27 m^2/m^2 (AWI-ESM1-1- LR) to 2.61 m^2/m^2 (MRI-ESM2-0), with an MME of 1.65 m^2/m^2 higher than observations), mainly due to the overestimation of LAI in non-forested vegetated areas.

Focusing on the two C4MIP experiments, they both have similar LAI values at about 700ppm, but their values at other CO_2 concentrations differ. For instance, at preindustrial CO_2, CESM1 (blue solid line) has a higher amount of leaf area (about 2 m^2/m^2) than CESM2 (green line) (about 1.4 m^2/m^2), but at higher CO_2 levels (> 800ppm), these results are reversed, with CESM2 surpassing 3 m^2/m^2 by the end of the simulation. Over the range of CO_2 concentrations that overlap the near present-day observations, CESM1 (thick solid blue line with crosses) has weaker LAI sensitivity to CO_2 (i.e., less steep slope) than CESM2 (thick solid green line with crosses) and is more closely aligned with the observations (thick solid grey lines with crosses). However, across a broader range of observations evaluated in Chen et al. (2019) (Figure S17), it is more difficult to distinguish which model version compares better. This large observational range results, in part, from differences in the algorithms used to estimate LAI and from differences in time periods assessed, the latter of which can be strongly influenced by interannual variability, and thus, longer observational records may be needed. Overall, these results demonstrate that accurate leaf area sensitivity is just as, or potentially more, important as

accurate leaf area values at specific CO_2 concentrations for capturing leaf area influences on the climate. Therefore, there is a continuing need to better constrain plant responses and their sensitivities to changes in CO_2 in order to improve future hydroclimate change assessments.

CHAPTER 4

DISCUSSION AND CONCLUSIONS

Rising CO_2 concentrations impact many aspects of the climate system, including all components of the hydrological cycle. Using several experiments with CESM versions 1 and 2, we focus on understanding the role of plant CO_2 physiological responses, particularly leaf area and stomatal conductance, and their influences on changes to the global hydroclimate. We find that leaf area changes play an important role in controlling the magnitude of the overall plant effects through the modulation of canopy evaporation and the resulting influence on total water fluxes. We quantify this role using controlled simulations within a single modeling framework and then apply our process level understanding to assess the reason for the differences across the model versions. While the leaf area response cannot solely explain the differences between the CESM1 and CESM2 C4MIP phys-only experiments, the experiments still exhibit similar changes in globally averaged total evaporation at elevated CO_2 as seen in the CESM2 fixed and dynamic leaf area phys-only runs. In particular, total evaporation decreases less with leaf area growth in the CESM2 C4MIP and dynamic simulations leading to smaller changes in globally averaged runoff and precipitation.

One important note is that the leaf area response cannot be completely separated from the stomatal conductance response with the simulations analyzed here. For instance, the effects of stomatal conductance on transpiration are partially influenced by leaf area changes (i.e., increased leaf area increases the number of stomata), so the changes in the dynamic run include

coupling between these two effects. Similarly, changes in one component of total evaporation can modulate the evaporative demand experienced by the other components, so there are small changes in canopy and soil evaporation even with fixed LAI. Other mechanisms, such as the influence of leaf shading of the soil surface, may also play a role but are not isolated in this study. However, the simulations still allow for an indirect quantification of the added leaf area response in the context of the stomatal conductance response. When comparing the two responses, we find that leaf area most strongly drives increases in canopy evaporation, while stomatal conductance most strongly drives decreases in transpiration.

Compared to observations, all of the simulations in this study overestimate the satellite-derived global mean leaf area, but biases are much larger in the CESM1 C4MIP and historical simulations than in the CESM2 C4MIP and historical simulations. Leaf area sensitivities to rising CO_2 also vary across the model versions. CESM1 is more in line with the weaker sensitivities observed in AVHRR and AVH15C1, but CESM2 is not outside the range from other observation-based products in the literature (e.g., Chen et al., 2019). These differences in LAI values and sensitivities further impact related carbon and land-atmosphere interactions, highlighting the ongoing uncertainty in, and the need to better constrain, the ways in which simulated plants respond to changes in CO_2 and the climate. And while we demonstrate that the leaf area response to CO_2 is an important factor in changes to the hydrological cycle, it is not the only process in land-atmosphere coupling that needs to be better constrained (e.g., soil hydrology likely also plays a role in the differences in runoff generation between the model versions).

It is also worth noting that the simulations in this study are idealized and thus, do not capture all the anthropogenically-driven changes to the earth system, and the experiments have different designs and configurations. For instance, the evolution of CO_2 is different in the C4MIP

experiments than in the fixed and dynamic runs, and CESM1 and CESM2 represent plant carbon allocation differently. Additionally, natural variability can influence the results, so we average over different lengths of time across the experiments in order to capture the CO_2 signals. However, despite these differences, the conclusions are robust across these different experiments, and we find qualitatively similar impacts of leaf area changes on overall plant physiology. Furthermore, when we assess the more realistic historical and ScenarioMIP simulations that include the anthropogenetic forcings, we find that the magnitudes and spatial patterns of the biases and sensitivities are nearly the same as the idealized simulations, suggesting that the mechanisms in the idealized CO_2-only simulations strongly influence widely-used 21st century climate projections.

Moving forward, it is useful to assess the role of leaf area changes in the context of other factors and processes that may influence its contribution to plant physiological effects, such as land use and land cover changes; nutrient availability and associated stresses; changes in plant height, overhead canopy, or leaf thickness (Kovenock & Swann, 2018); dynamic changes to plant type and maturity; pests and diseases; and plant responses over fast (i.e., within a growing season) and slow (i.e., years to decades) timescales (McDermid et al., 2021). It would also be useful to focus on specific regions, looking beyond global averages, because the tropics dominate the global LAI signal, and changes in the hydroclimate can depend on local background climate conditions (e.g., temperature; precipitation amount, frequency, type, and distribution; regional topography). Additionally, observations tend to underestimate LAI in biomes with densely vegetated cover, so focusing on regions with better observational performance could provide more realistic comparisons to simulated LAI. Regional analysis would also enable more direct use of surface-based measurements and experiments, such as the

Free Air CO_2 Enrichment (FACE) experiments (Norby & Zak, 2011), which could help constrain some of the limitations of leaf area derived from satellite-based products.

Overall, this work highlights that improving hydroclimate simulations and projections depends not only on atmospheric processes but also on the land-surface and the representation of vegetation. There is strong coupling between carbon and water cycling that is controlled by a variety of plant-related processes and their influences on water fluxes, which can play significant roles in the evolution of the hydroclimate and the overall earth climate system.

REFERENCES

Allan, R. P., Barlow, M., Byrne, M. P., Cherchi, A., Douville, H., Fowler, H. J., et al. (2020). Advances in understanding large-scale responses of the water cycle to climate change. *Ann. N.Y. Acad. Sci.*, *1472*, 49-75. https://doi.org/10.1111/nyas.14337

Arias, P.A., N. Bellouin, E. Coppola, R.G. Jones, G. Krinner, J. Marotzke, V. Naik, M.D. Palmer, G.-K. Plattner, J. Rogelj, M. Rojas, J. Sillmann, T. Storelvmo, P.W. Thorne, B. Trewin, K. Achuta Rao, B. Adhikary, R.P. Allan, K. Armour, … K. Zickfeld, 2021: Technical Summary. In *Climate Change 2021: The Physical Science Basis. Contribution of Working Group I to the Sixth Assessment Report of the Intergovernmental Panel on Climate Change* [Masson-Delmotte, V., P. Zhai, A. Pirani, S.L. Connors, C. Péan, S. Berger, N. Caud, Y. Chen, L. Goldfarb, M.I. Gomis, M. Huang, K. Leitzell, E. Lonnoy, J.B.R. Matthews, T.K. Maycock, T. Waterfield, O. Yelekçi, R. Yu, and B. Zhou (eds.)]. Cambridge University Press, Cambridge, United Kingdom and New York, NY, USA, pp. 33−144. doi:10.1017/9781009157896.002.

Ball, J. T., Woodrow, I. E., & Berry, J. A. (1987). A model predicting stomatal conductance and its contribution to the control of photosynthesis under different environmental conditions. In J. Biggins (Ed.), *Progress in photosynthesis research*, 221–224. Netherlands: Springer. https://doi.org/10.1007/978-94-017-0519-6_48

Berg, A., & McColl, K. A. (2021). No projected global drylands expansion under greenhouse warming. *Nature Climate Change, 11*(4), 331–337. https://doi.org/10.1038/s41558-021-01007-8

Brodribb, T.J., Sussmilch, F., & McAdam, S.A.M. (2020). From reproduction to production, stomata are the master regulators. *Plant J*, *101*, 756-767. https://doi.org/10.1111/tpj.14561

Chen, J. M., Ju, W., Ciais, P., Viovy, N., Liu, R., Liu, Y., & Lu, X. (2019). Vegetation structural change since 1981 significantly enhanced the terrestrial carbon sink. *Nature Communications 2019 10:1*, *10*(1), 1–7. https://doi.org/10.1038/s41467-019-12257-8

Claverie, M., Matthews, J. L., Vermote, E. F., Justice, C. O., Zhao, X., Yang, W., John, V., Lu, H., Knapp, K., Huete, A. R., & Thenkabail, P. S. (2016). A 30+ Year AVHRR LAI and FAPAR Climate Data Record: Algorithm Description and Validation. *Remote Sensing 2016, Vol. 8, Page 263*, *8*(3), 263. https://doi.org/10.3390/RS8030263

Cornish, A. E., G. J. Kooperman, A. J. Grundstein, C. B. Skinner, & A. L. S. Swann (2023, in-prep). The Impact of Plant-Physiological Responses to Rising CO_2 on Humidity Driven Extreme Heat.

Danabasoglu, G., Lamarque, J.-F., Bacmeister, J., Bailey, D. A., DuVivier, A. K., Edwards, J., et al. (2020). The Community Earth System Model Version 2 (CESM2). *Journal of Advances in Modeling Earth Systems*, *12*. https://doi.org/10.1029/2019MS001916

Douville, H., K. Raghavan, J. Renwick, R.P. Allan, P.A. Arias, M. Barlow, R. Cerezo-Mota, A. Cherchi, T.Y. Gan, J. Gergis, D. Jiang, A. Khan, W. Pokam Mba, D. Rosenfeld, J. Tierney, and O. Zolina, 2021: Water Cycle Changes. In Climate Change 2021: The Physical Science Basis. Contribution of Working Group I to the Sixth Assessment Report of the Intergovernmental Panel on Climate Change [Masson-Delmotte, V., P. Zhai, A. Pirani, S.L. Connors, C. Péan, S. Berger, N. Caud, Y. Chen, L. Goldfarb, M.I. Gomis, M. Huang, K. Leitzell, E. Lonnoy, J.B.R. Matthews, T.K. Maycock, T. Waterfield, O. Yelekçi, R. Yu,

and B. Zhou (eds.)]. Cambridge University Press, Cambridge, United Kingdom and New York, NY, USA, pp. 1055–1210, doi:10.1017/9781009157896.010.

Eyring, V., Bony, S., Meehl, G. A., Senior, C. A., Stevens, B., Stouffer, R. J., & Taylor, K. E. (2016). Overview of the Coupled Model Intercomparison Project Phase 6 (CMIP6) experimental design and organization. *Geoscientific Model Development*, *9*, 1937–1958. https://doi.org/10.5194/gmd-9-1937-2016.

Fowler, M. D., Kooperman, G. J., Randerson, J. T., & Pritchard, M. S. (2019). The effect of plant physiological responses to rising CO2 on global streamflow. *Nature Climate Change*, *9*(11), 873–879. https://doi.org/10.1038/s41558-019-0602-x

Frank, D. C., Poulter, B., Saurer, M., Esper, J., Huntingford, C., Helle, G., et al. (2015). Water-use efficiency and transpiration across Euro-pean forests during the Anthropocene. *Nature Climate Change, 5*(6), 579–583. https://doi.org/10.1038/nclimate2614

Guerrieri, R., Belmecheri, S., Ollinger, S. V., Asbjornsen, H., Jennings, K., Xiao, J., et al. (2019). Disentangling the role of photosynthesis and stomatal conductance on rising forest water-use efficiency. *Proceedings of the National Academy of Sciences of the United States of America*, *116*(34), 16909–16914. https://doi.org/10.1073/pnas.1905912116

Holben, B. N. (1986). Characteristics of maximum-value composite images from temporal AVHRR data. *International Journal of Remote Sensing*, *7*(11), 1417–1434. https://doi.org/10.1080/01431168608948945

Hong, T., Dong, W., Ji, D. Dai, T., Yang, S., & Wei, T. (2019). The response of vegetation to rising CO_2 concentrations plays an important role in future changes in the hydrological cycle. *Theor Appl Climatol 136*, 135–144. https://doi.org/10.1007/s00704-018-2476-7

Jiang, M., Medlyn, B. E., Drake, J. E., Duursma, R. A., Anderson, I. C., Barton, C. V. M., Boer, M. M., Carrillo, Y., Castañeda-Gómez, L., Collins, L., Crous, K. Y., de Kauwe, M. G., dos Santos, B. M., Emmerson, K. M., Facey, S. L., Gherlenda, A. N., Gimeno, T. E., Hasegawa, S., Johnson, S. N., … Ellsworth, D. S. (2020). The fate of carbon in a mature forest under carbon dioxide enrichment. *Nature, 580*(7802), 227–231. https://doi.org/10.1038/s41586-020-2128-9

Jiang, M., Kelly, J. W. G., Atwell, B. J., Tissue, D. T., & Medlyn, B. E. (2021). Drought by CO2 interactions in trees: a test of the water savings mechanism. *New Phytologist*, *230*(4), 1421–1434. https://doi.org/10.1111/NPH.17233

Jones, C. D., Arora, V., Friedlingstein, P., Bopp, L., Brovkin, V., Dunne, J., et al. (2016). C4MIP – The Coupled Climate–Carbon Cycle Model Intercomparison Project: experimental protocol for CMIP6. *Geosci. Model Dev., 9*, 2853-2880. https://doi.org/10.5194/gmd-9-2853-2016

Kooperman, G. J., Chen, Y., Hoffman, F. M., Koven, C. D., Lindsay, K., Pritchard, M. S., Swann, A. L. S., & Randerson, J. T. (2018a). Forest response to rising CO_2 drives zonally asymmetric rainfall change over tropical land. *Nature Climate Change*, *8*(5), 434–440. https://doi.org/10.1038/s41558-018-0144-7

Kooperman, G. J., Fowler, M. D., Hoffman, F. M., Koven, C. D., Lindsay, K., Pritchard, M. S., et al. (2018b). Plant physiological responses to rising CO_2 modify simulated daily runoff intensity with implications for global-scale flood risk assessment. *Geophysical Research Letters*, *45*(12), 457–12, 466. https://doi.org/10.1029/2018GL079901

Kovenock, M., & Swann, A. L. S. (2018). Leaf trait acclimation amplifies simulated climate warming in response to elevated carbon dioxide. *Global Biogeochemical Cycles, 32*(10), 1437–1448. https://doi.org/10.1029/2018GB005883

Lawrence, D. M., Oleson, K. W., Flanner, M. G., Thornton, P. E., Swenson, S. C., Lawrence, P. J., et al. (2011). Parameterization improvements and functional and structural advances in version 4 of the Community Land Model. *Journal of Advances in Modeling Earth Systems*, *3*, M03001. https://doi.org/10.1029/2011MS000045

Lawrence, D. M., Fisher, R., Koven, C., Oleson, K., Swenson, S., Vertenstein, M., et al. (2018). Technical Description of version 5.0 of the Community Land Model (CLM) (NCAR Technical Note). Boulder, CO: National Center for Atmospheric Research.

Lawrence, D. M., Fisher, R. A., Koven, C. D., Oleson, K. W., Swenson, S. C., Bonan, G., et al. (2019). The Community Land Model version 5: Description of new features, benchmarking, and impact of forcing uncertainty. *Journal of Advances in Modeling Earth Systems*, *11*, 4245-4287. https://doi-org.cuucar.idm.oclc.org/10.1029/2018MS001583.

Lawson, T. and Vialet-Chabrand, S. (2019). Speedy stomata, photosynthesis and plant water use efficiency. *New Phytol*, *221*, 93-98. https://doi.org/10.1111/nph.15330

Lee, J. -Y., J. Marotzke, G. Bala, L. Cao, S. Corti, J.P. Dunne, F. Engelbrecht, E. Fischer, J.C. Fyfe, C. Jones, A. Maycock, J. Mutemi, O. Ndiaye, S. Panickal, and T. Zhou, 2021: Future Global Climate: Scenario-Based Projections and Near- Term Information. In *Climate Change 2021: The Physical Science Basis. Contribution of Working Group I to the Sixth Assessment Report of the Intergovernmental Panel on Climate Change* [Masson-Delmotte, V., P. Zhai, A. Pirani, S.L. Connors, C. Péan, S. Berger, N. Caud, Y. Chen, L. Goldfarb, M.I. Gomis, M. Huang, K. Leitzell, E. Lonnoy, J.B.R. Matthews, T.K. Maycock, T.

Waterfield, O. Yelekçi, R. Yu, and B. Zhou (eds.)]. Cambridge University Press, Cambridge, United Kingdom and New York, NY, USA, pp. 553–672, doi:10.1017/9781009157896.006.

Lemordant, L., Gentine, P., Swann, A. S., Cook, B. I., & Scheff, J. (2018). Critical impact of vegetation physiology on the continental hydrologic cycle in response to increasing CO2. *Proceedings of the National Academy of Sciences of the United States of America*, *115*(16), 4093–4098. https://doi.org/10.1073/pnas.1720712115

Lian, X., Piao, S., Chen, A., Huntingford, C., Fu, B., Li, L. Z. X., Huang, J., Sheffield, J., Berg, A. M., Keenan, T. F., McVicar, T. R., Wada, Y., Wang, X., Wang, T., Yang, Y., & Roderick, M. L. (2021). Multifaceted characteristics of dryland aridity changes in a warming world. *Nature Reviews Earth & Environment 2021 2:4*, *2*(4), 232–250. https://doi.org/10.1038/s43017-021-00144-0

Lindsay, K., Bonan, G. B., Doney, S. C., Hoffman, F. M., Lawrence, D. M., Long, M. C., et al. (2014). Preindustrial-Control and Twentieth-Century Carbon Cycle Experiments with the Earth System Model CESM1(BGC). *Journal of Climate*, *27*(24), 8981-9005. https://journals.ametsoc.org/view/journals/clim/27/24/jcli-d-12-00565.1.xml

Mankin, J. S., Smerdon, J. E., Cook, B. I., Williams, A. P., & Seager, R. (2017). The Curious Case of Projected Twenty-First-Century Drying but Greening in the American West. *Journal of Climate*, *30*(21), 8689–8710. https://doi.org/10.1175/JCLI-D-17-0213.1

Mankin, J. S., Seager, R., Smerdon, J. E., Cook, B. I., Williams, A. P., & Horton, R. M. (2018). Blue Water Trade-Offs With Vegetation in a CO2-Enriched Climate. *Geophysical Research Letters*, *45*(7), 3115–3125. https://doi.org/10.1002/2018GL077051

Mankin, J. S., Seager, R., Smerdon, J. E., Cook, B. I., & Williams, A. P. (2019). Mid-latitude freshwater availability reduced by projected vegetation responses to climate change. *Nature Geoscience 2019 12:12*, *12*(12), 983–988. https://doi.org/10.1038/s41561-019-0480-x

McDermid, S. S., Cook, B. I., de Kauwe, M. G., Mankin, J., Smerdon, J. E., Williams, A. P., et al. (2021). Disentangling the Regional Climate Impacts of Competing Vegetation Responses to Elevated Atmospheric CO2. *Journal of Geophysical Research: Atmospheres*, *126*(5), 1–23. https://doi.org/10.1029/2020JD034108

Medlyn, B. E., Duursma, R. A., Eamus, D., Ellsworth, D. S., Prentice, I. C., Barton, C. V. M., et al. (2011). Reconciling the optimal and empirical approaches to modeling stomatal conductance. *Global Change Biology, 17*(6), 2134-2144. https://doi.org/10.1111/j.1365-2486.2010.02375.x

Montané, F., Fox, A. M., Arellano, A. F., MacBean, N., Ross A., M., Dye, A., Bishop, D. A., Trouet, V., Babst, F., Hessl, A. E., Pederson, N., Blanken, P. D., Bohrer, G., Gough, C. M., Litvak, M. E., Novick, K. A., Phillips, R. P., Wood, J. D., & Moore, D. J. P. (2017). Evaluating the effect of alternative carbon allocation schemes in a land surface model (CLM4.5) on carbon fluxes, pools, and turnover in temperate forests. *Geoscientific Model Development*, *10*(9), 3499–3517. https://doi.org/10.5194/GMD-10-3499-2017

Neale, R. B., Richterm, J. H., Conley, A. J., Park, S., Lauritzen, P. H., Gettelman, A., et al. (2010). Description of the NCAR Community Atmosphere Model (CAM 4.0) (NCAR Technical Note: NCAR/TN-485+STR). Boulder, CO: National Center for Atmospheric Research.

Neely, R. R., Marsh, D. R., Smith, K. L., Davis, S. M., & Polvani, L. M. (2014). Biases in southern hemisphere climate trends induced by coarsely specifying the temporal resolution of stratospheric ozone. *Geophysical Research Letters*, *41*(23), 8602–8610. https://doi.org/10.1002/2014GL061627.

Negrón-Juárez, R. I., Koven, C. D., Riley, W. J., Knox, R. G., & Chambers, J. Q. (2015). Observed allocations of productivity and biomass, and turnover times in tropical forests are not accurately represented in CMIP5 Earth system models. *Environmental Research Letters*, *10*(6), 064017. https://doi.org/10.1088/1748-9326/10/6/064017

Norby, R. J. and Zak, D. R. (2011). Ecological lessons from free-air CO2 enrichment (FACE) experiments. *Annual Review of Ecology, Evolution and Systematics, 42*, 181–203. https://doi.org/10.1146/annurev-ecolsys-102209-144647

Oleson, K. W., Lawrence, D. M., Bonan, G. B., Flanner, M. G., Kluzek, E., Lawrence, P. J., et al. (2010). Technical Description of version 4.0 of the Community Land Model (CLM) (NCAR Technical Note: NCAR/TN-478+STR). Boulder, CO: National Center for Atmospheric Research.

O'Neill, B. C., Tebaldi, C., van Vuuren, D. P., Eyring, V., Friedlingstein, P., Hurtt, G., et al. (2016). The Scenario Model Intercomparison Project (ScenarioMIP) for CMIP6. *Geoscientific Model Development*, *9*(9), 3461–3482. https://doi.org/10.5194/GMD-9-3461-2016

Prentice, I. C., Farquhar, G. D., Fasham, M. J. R., Goulden, M. L., Heimann, M., Jaramillo, V. J., et al. (2001). The carbon cycle and atmospheric carbon dioxide. In J. T. Houghton, Y. Ding, D. J. Griggs, M. Noguer, P. J. V. D. Linden, X. Dai, K. Maskell, & C. A. Johnson (Eds.), *Climate Change 2001: The Scientific Basis*, 183-237. Cambridge University Press.

Rogers, A., Medlyn, B. E., Dukes, J. S., Bonan, G., von Caemmerer, S., Dietze, M. C., et al. (2017). A roadmap for improving the representation of photosynthesis in Earth system models. *New Phytol*, *213*(1), 22-42. https://doi.org/10.1111/nph.14283

Singh, A., Kumar, S., Akula, S., Lawrence, D. M., & Lombardozzi, D. L. (2020). Plant Growth Nullifies the Effect of Increased Water-Use Efficiency on Streamflow Under Elevated CO2 in the Southeastern United States. *Geophysical Research Letters*, *47*(4), 1–10. https://doi.org/10.1029/2019GL086940

Skinner, C. B., Poulsen, C. J., Chadwick, R., Diffenbaugh, N. S., & Fiorella, R. P. (2017). The role of plant CO2 physiological forcing in shaping future daily-scale precipitation. *Journal of Climate*, *30*(7), 2319–2340. https://doi.org/10.1175/JCLI-D-16-0603.1

Song, X., Wang, D. Y., Li, F., & Zeng, X. D. (2020). Evaluating the performance of CMIP6 Earth system models in simulating global vegetation structure and distribution. *Advances in Climate Change Research*, *12*(4), 584–595. https://doi.org/10.1016/J.ACCRE.2021.06.008

Swann, A. L. S., Hoffman, F. M., Koven, C. D., & Randerson, J. T. (2016). Plant responses to increasing CO2 reduce estimates of climate impacts on drought severity. *Proceedings of the National Academy of Sciences of the United States of America*, *113*(36), 10019–10024. https://doi.org/10.1073/pnas.1604581113

Taylor, K. E., Stouffer, R. J., & Meehl, G. A. (2012). An Overview of CMIP5 and the Experiment Design. *Bulletin of the American Meteorological Society*, *93*(4), 485-498. https://journals.ametsoc.org/view/journals/bams/93/4/bams-d-11-00094.1.xml

UCAR. (2017). *Welcome to the CAM documentation*. https://ncar.github.io/CAM/doc/build/html/index.html

van Vuuren, D. P., Edmonds, J., Kainuma, M., Riahi, K., Thomson, A., Hibbard, K., et al. (2011). The representative concentration pathways: An overview. *Climatic Change*, *109*(1), 5–31. https://doi.org/10.1007/S10584-011-0148-Z/TABLES/4

Vermote, Eric; NOAA CDR Program. (2019): NOAA Climate Data Record (CDR) of AVHRR Leaf Area Index (LAI) and Fraction of Absorbed Photosynthetically Active Radiation (FAPAR), Version 5. NOAA National Centers for Environmental Information. https://doi.org/10.7289/V5TT4P69.

Wieder, W. R., Lawrence, D. M., Fisher, R. A., Bonan, G. B., Cheng, S. J., Goodale, C. L., Grandy, A. S., Koven, C. D., Lombardozzi, D. L., Oleson, K. W., & Thomas, R. Q. (2019). Beyond Static Benchmarking: Using Experimental Manipulations to Evaluate Land Model Assumptions. *Global Biogeochemical Cycles*, *33*(10), 1289–1309. https://doi.org/10.1029/2018GB006141

Zarakas, C. M., Swann, A. L. S., Laguë, M. M., Armour, K. C., & Randerson, J. T. (2020). Plant Physiology Increases the Magnitude and Spread of the Transient Climate Response to CO2 in CMIP6 Earth System Models. *Journal of Climate*, *33*(19), 8561–8578. https://doi.org/10.1175/JCLI-D-20-0078.1

Zhang, X., Zhang, Y., Ma, N., Kong, D., Tian, J., Shao, X., & Tang, Q. (2021). Greening-induced increase in evapotranspiration over Eurasia offset by CO_2-induced vegetational stomatal closure. *Environmental Research Letters*, *16*(12), 124008. https://doi.org/10.1088/1748-9326/AC3532

Zhang, X. Y., Jin, J., Zeng, X., Hawkins, C. P., Neto, A. A. M., & Niu, G. Y. (2022). The Compensatory CO_2 Fertilization and Stomatal Closure Effects on Runoff Projection From

2016–2099 in the Western United States. *Water Resources Research*, *58*(1). https://doi.org/10.1029/2021WR030046

Zhu, B., Huang, M., Cheng, Y., Xie, X., Liu, Y., Bisht, G., & Chen, X. (2021). Impact of Vegetation Physiology and Phenology on Watershed Hydrology in a Semiarid Watershed in the Pacific Northwest in a Changing Climate. *Water Resources Research*, *57*(3), 1–24. https://doi.org/10.1029/2020WR028394

APPENDIX A

RESULTS SECTION 1 SUPPLEMENTAL FIGURES

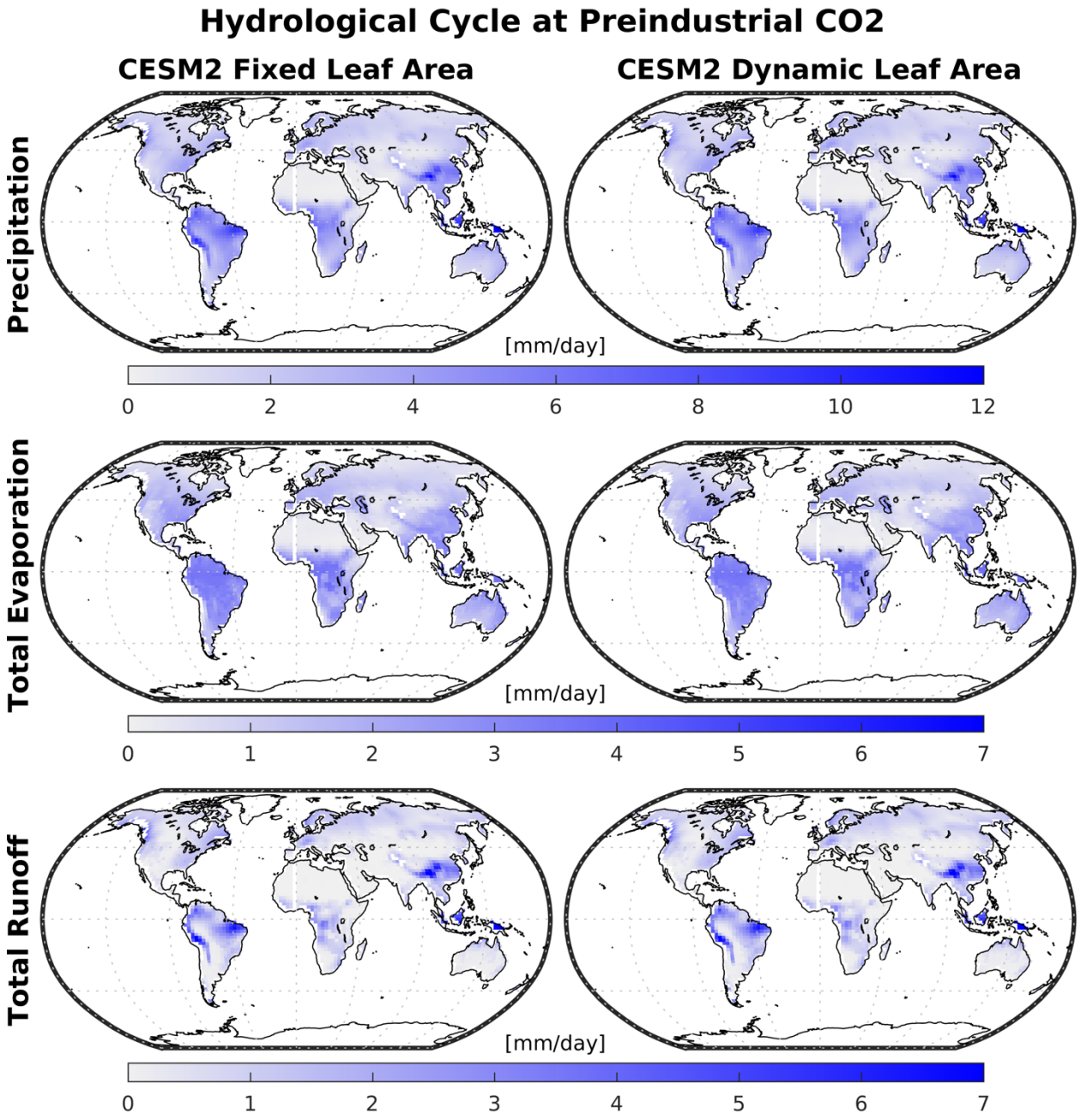

Figure S1. Precipitation, total evaporation, and total runoff at preindustrial CO_2 for CESM2 fixed [left column] and dynamic [right column] leaf area phys-only runs.

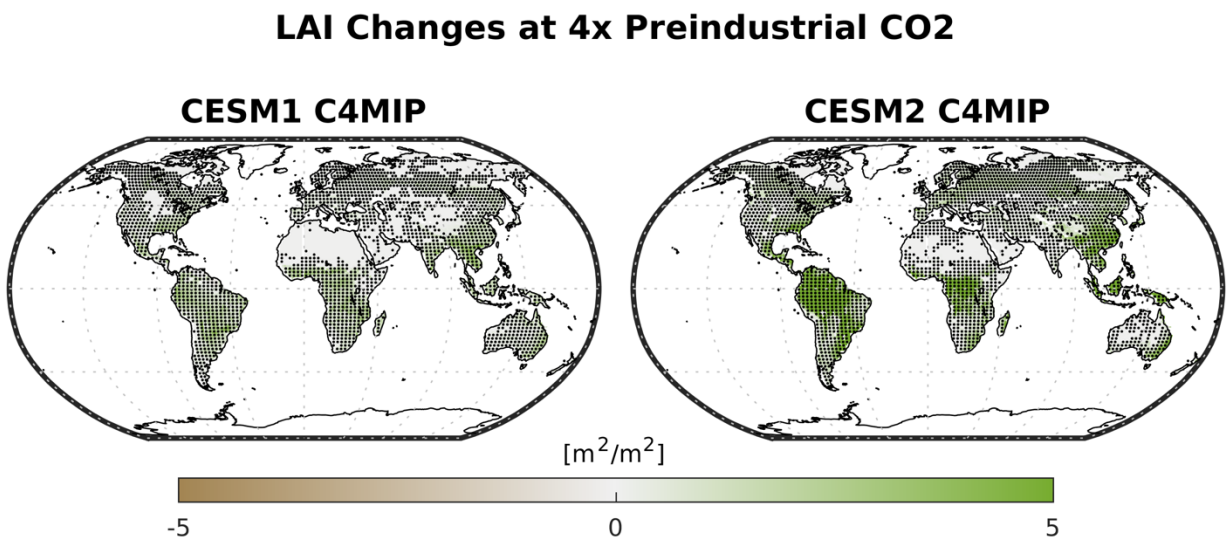

Figure S2. Changes in leaf area index between preindustrial CO_2 and 4x preindustrial CO_2 for CESM1 [left] and CESM2 [right] C4MIP phys-only experiments. Stippling represents 90% significance, calculated using a paired t-test and an alpha value of 0.1.

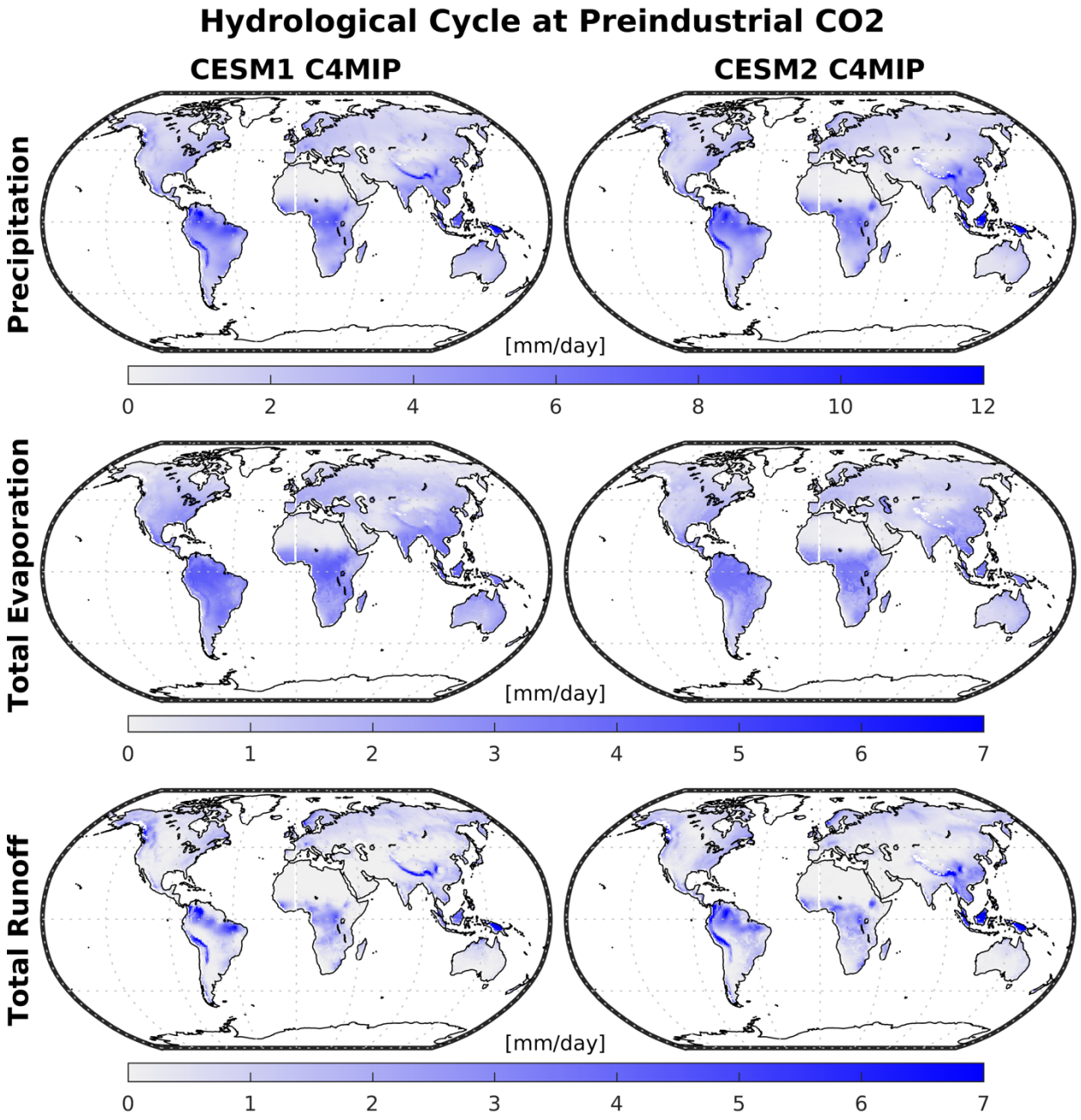

Figure S3. Precipitation, total evaporation, and total runoff at preindustrial CO_2 for CESM1 [left column] and CESM2 [right column] C4MIP phys-only experiments.

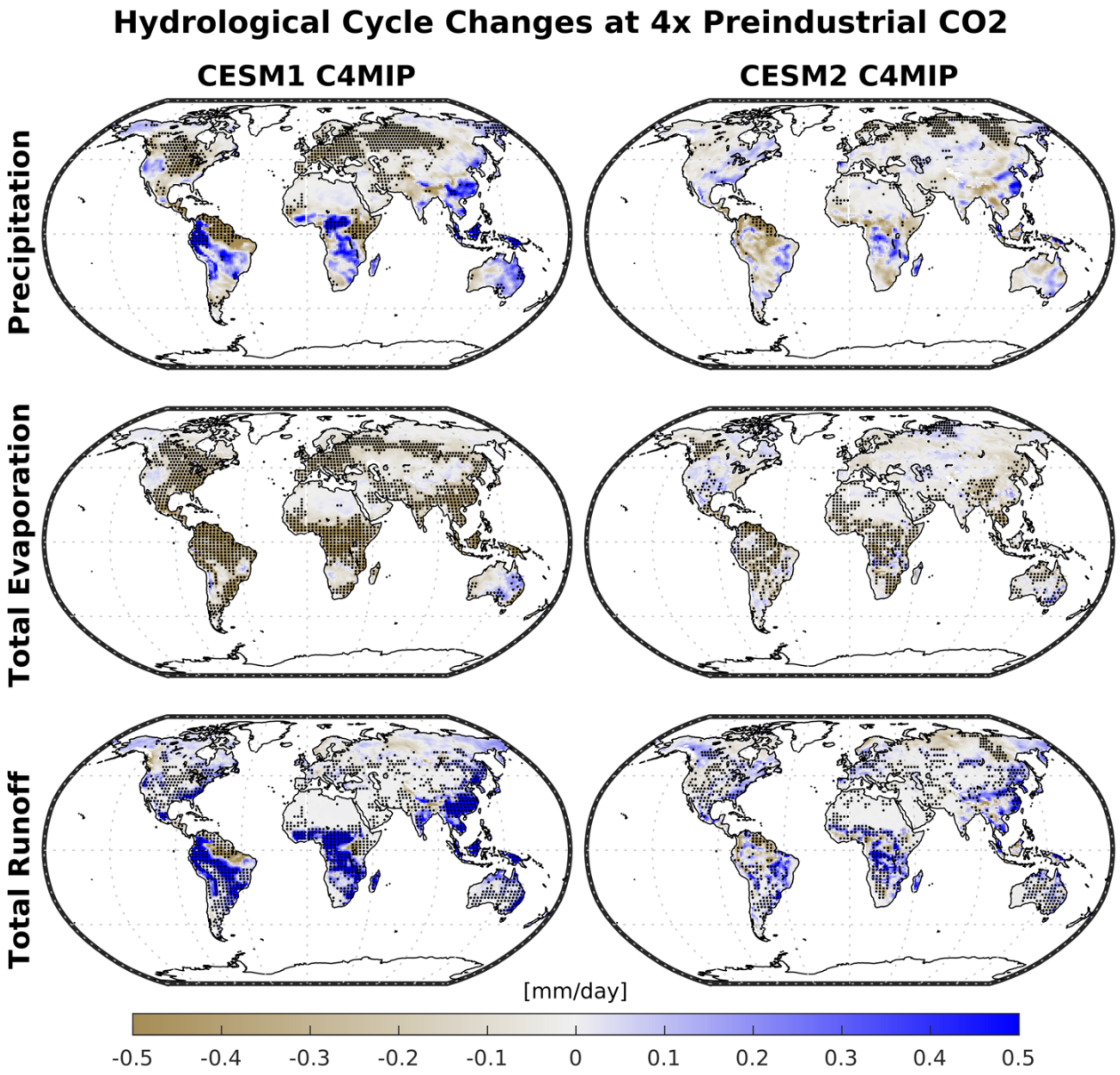

Figure S4. Changes in precipitation, total evaporation, and total runoff between preindustrial CO_2 and 4x preindustrial CO_2 for CESM1 [left column] and CESM2 [right column] C4MIP phys-only experiments. Stippling represents 90% significance, calculated using a paired t-test and an alpha value of 0.1.

APPENDIX B

RESULTS SECTION 2 SUPPLEMENTAL FIGURES

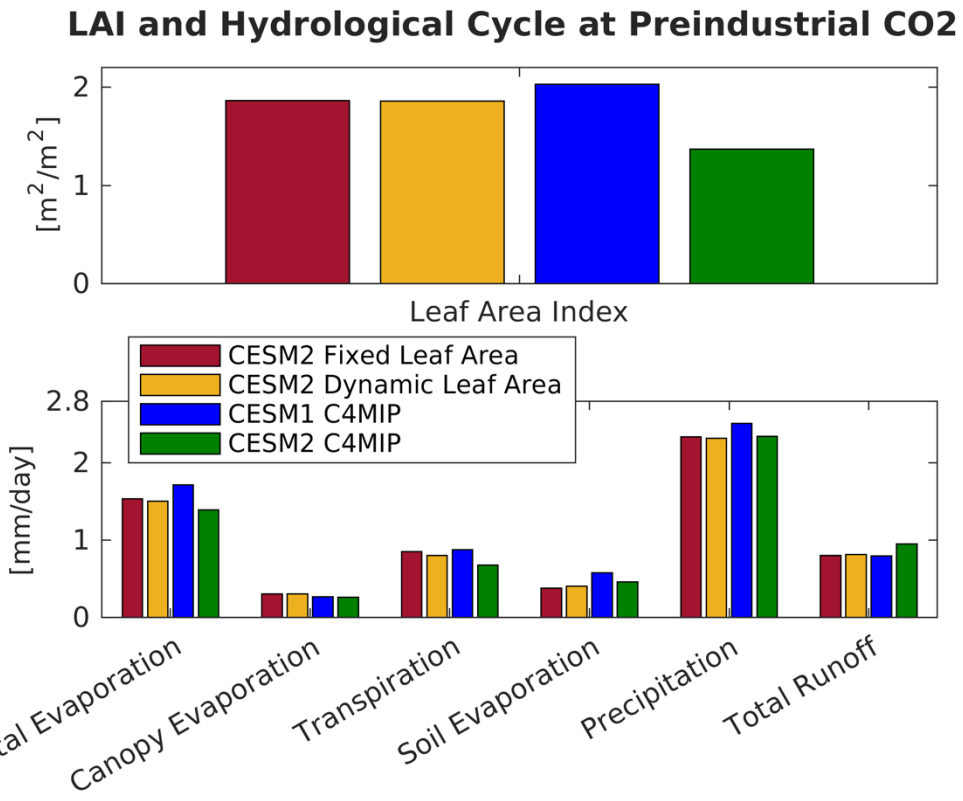

Figure S5. Global land averages (excluding glacier regions) of leaf area index, total evaporation, components of total evaporation (i.e., canopy evaporation, transpiration, and soil evaporation), precipitation, and total runoff at preindustrial CO_2 for CESM2 fixed [red bars] and dynamic [yellow bars] phys-only leaf area runs, and CESM1 [blue bars] and CESM2 [green bars] C4MIP phys-only experiments.

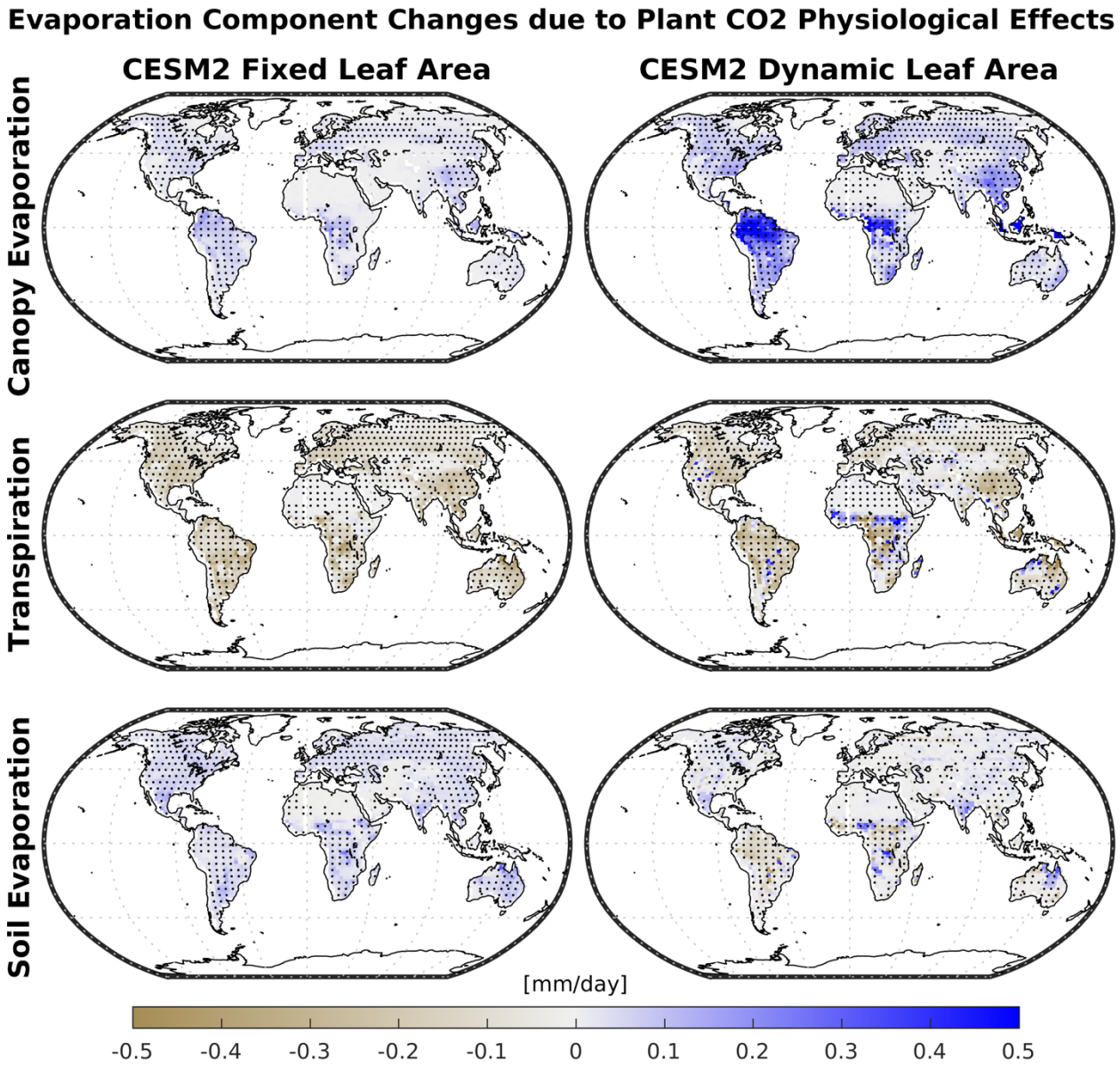

Figure S6. Changes in the components of total evaporation (i.e., canopy evaporation, transpiration, and soil evaporation) between preindustrial CO_2 and 2x preindustrial CO_2 for CESM2 fixed [left column] and dynamic [right column] leaf area phys-only runs. Stippling represents 90% significance, calculated using a paired t-test and an alpha value of 0.1.

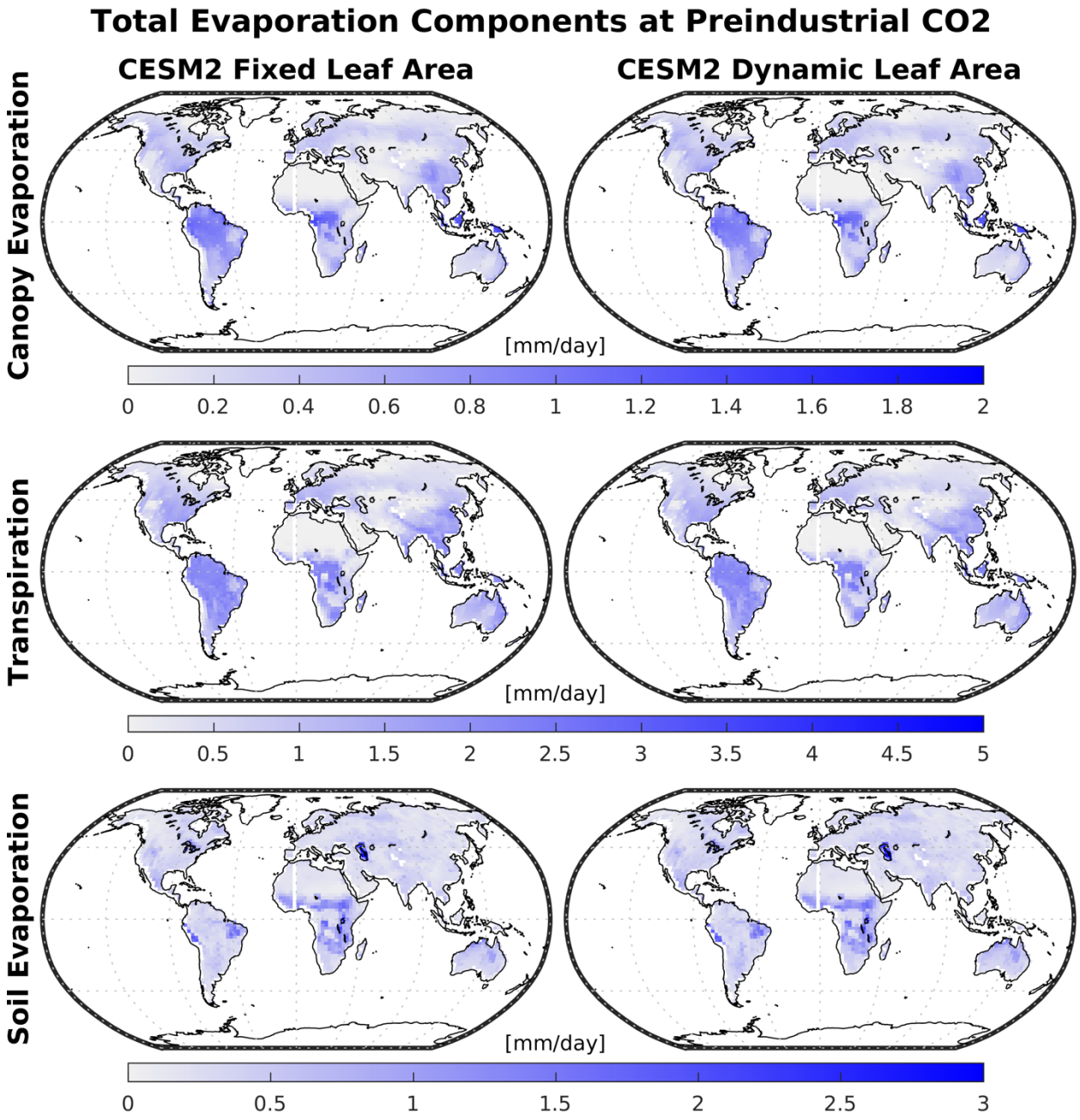

Figure S7. Components of total evaporation (i.e., canopy evaporation, transpiration, and soil evaporation) at preindustrial CO_2 for CESM2 fixed [left column] and dynamic [right column] leaf area phys-only runs.

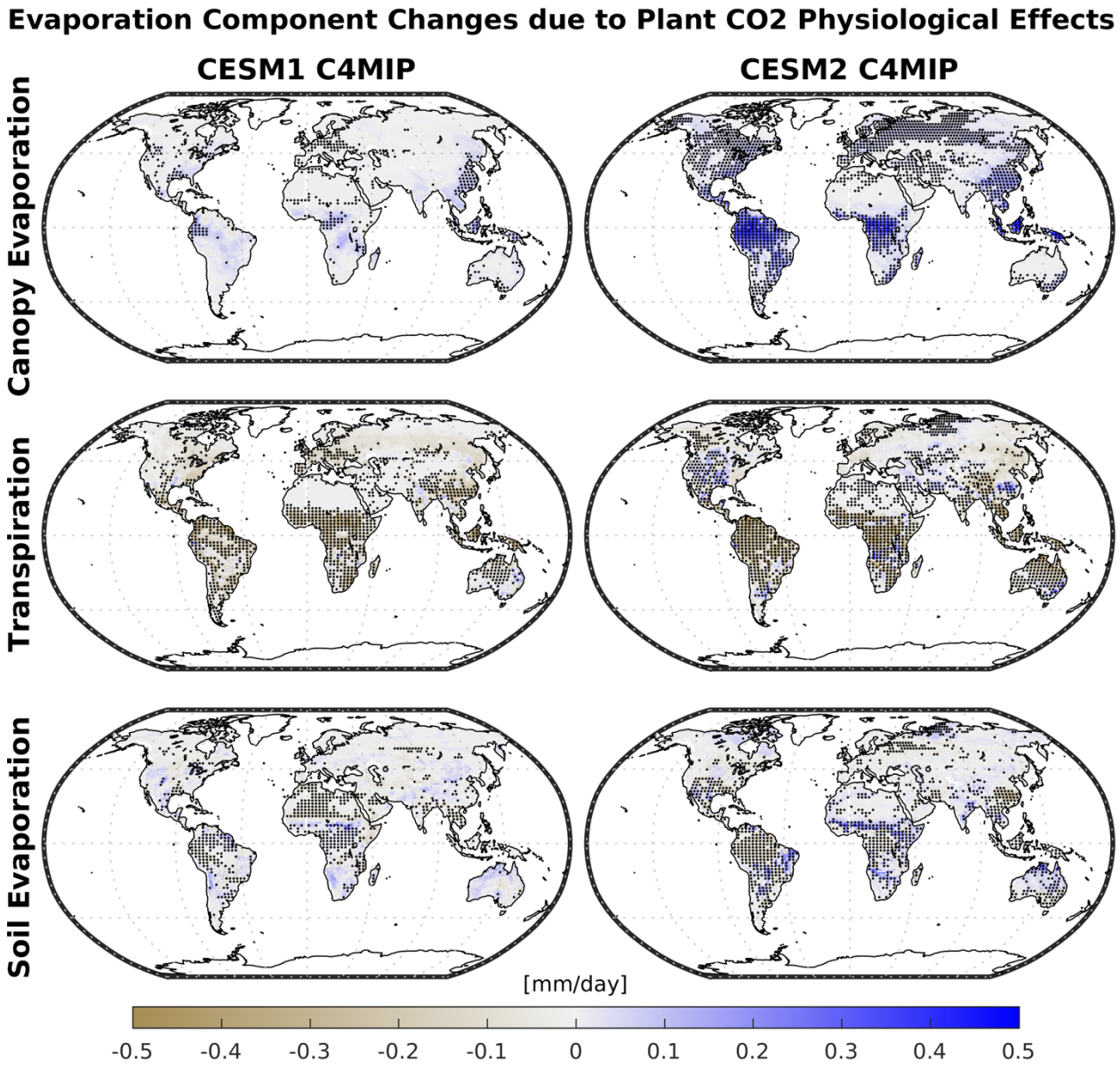

Figure S8. Changes in the components of total evaporation (i.e., canopy evaporation, transpiration, and soil evaporation) between preindustrial CO_2 and 2x preindustrial CO_2 for CESM1 [left column] and CESM2 [right column] C4MIP phys-only experiments. Stippling represents 90% significance, calculated using a paired t-test and an alpha value of 0.1.

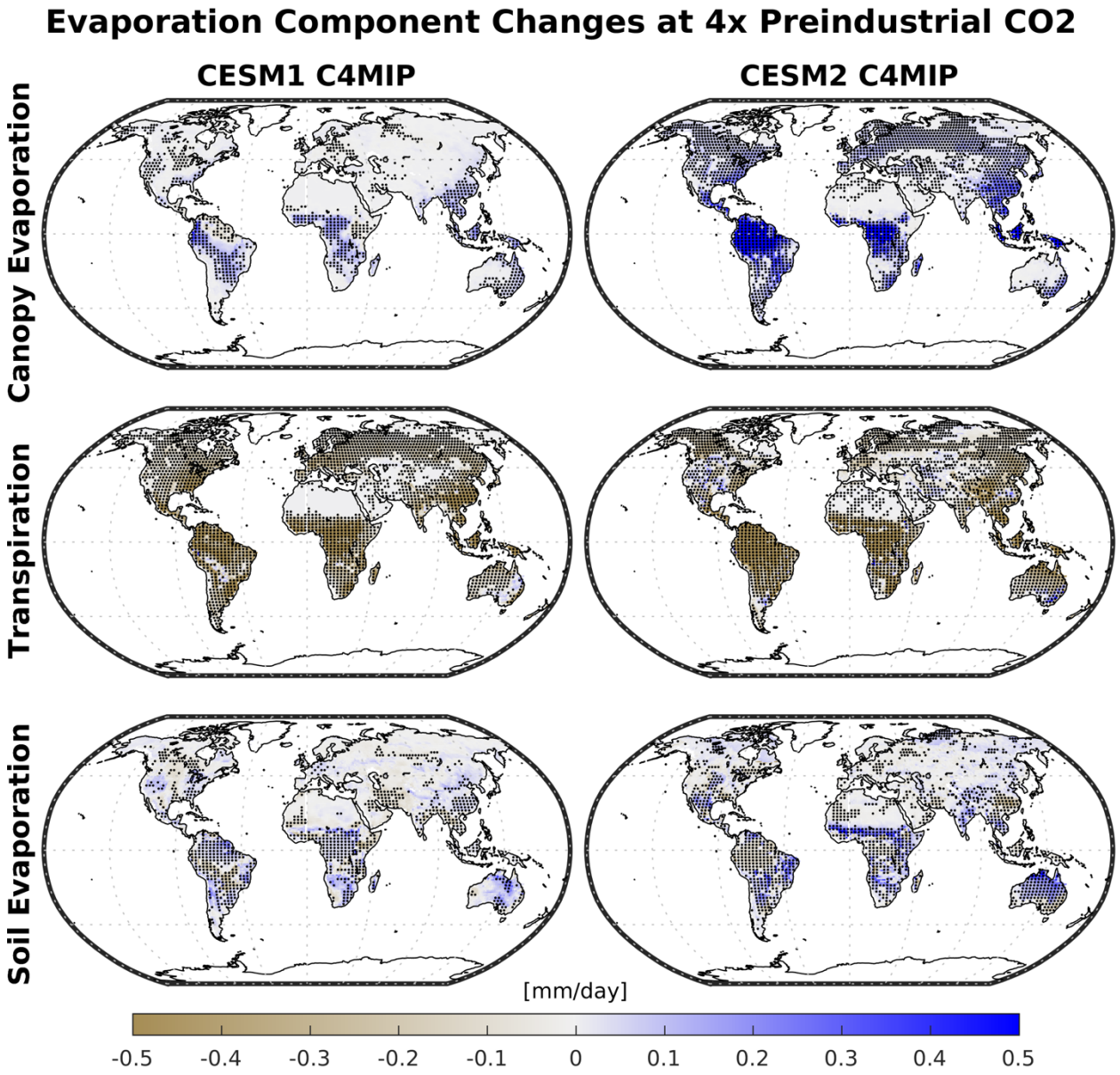

Figure S9. Changes in the components of total evaporation (i.e., canopy evaporation, transpiration, and soil evaporation) between preindustrial CO_2 and 4x preindustrial CO_2 for CESM1 [left column] and CESM2 [right column] C4MIP phys-only experiments. Stippling represents 90% significance, calculated using a paired t-test and an alpha value of 0.1.

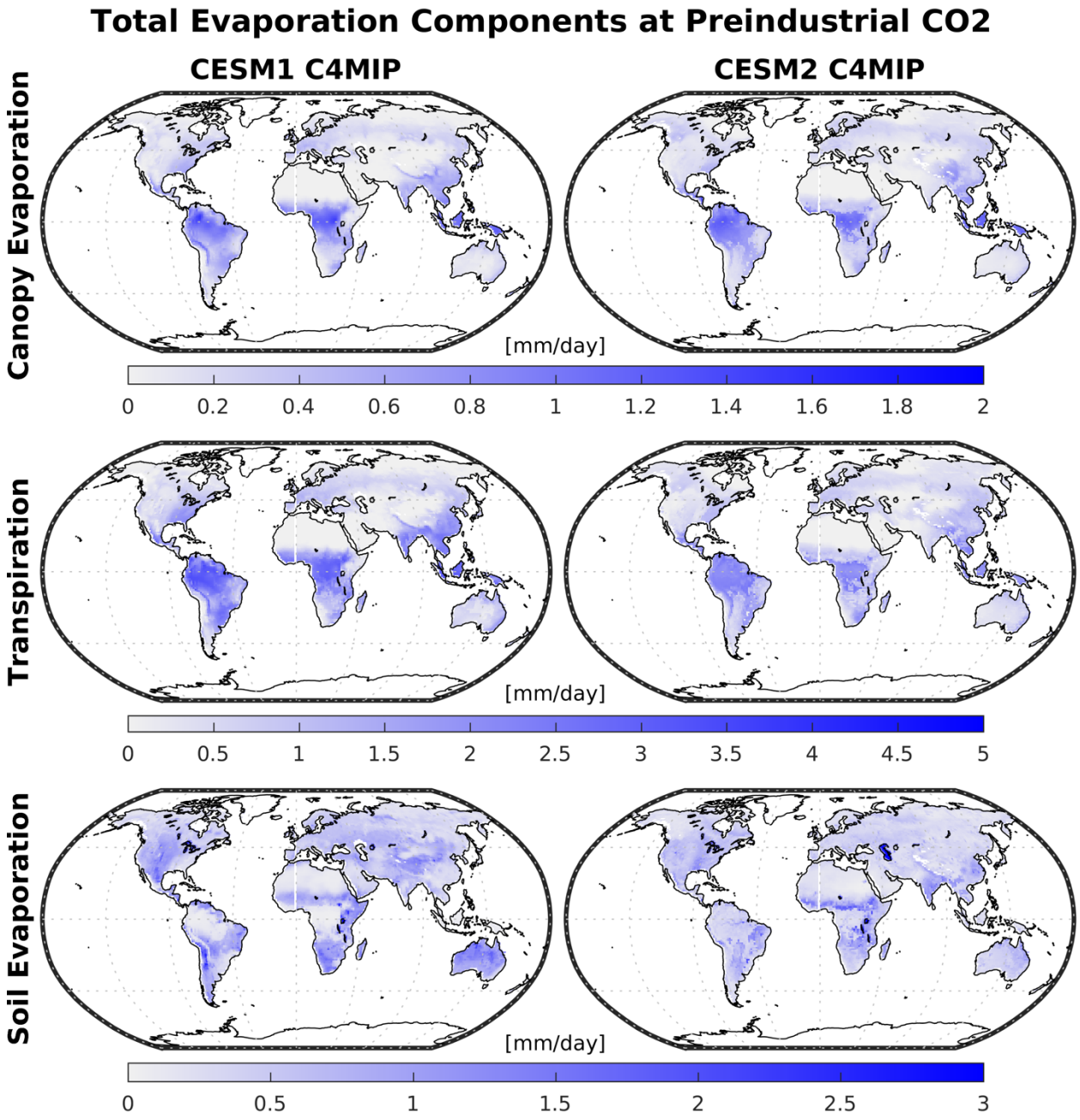

Figure S10. Components of total evaporation (i.e., canopy evaporation, transpiration, and soil evaporation) at preindustrial CO_2 for CESM1 [left column] and CESM2 [right column] C4MIP phys-only experiments.

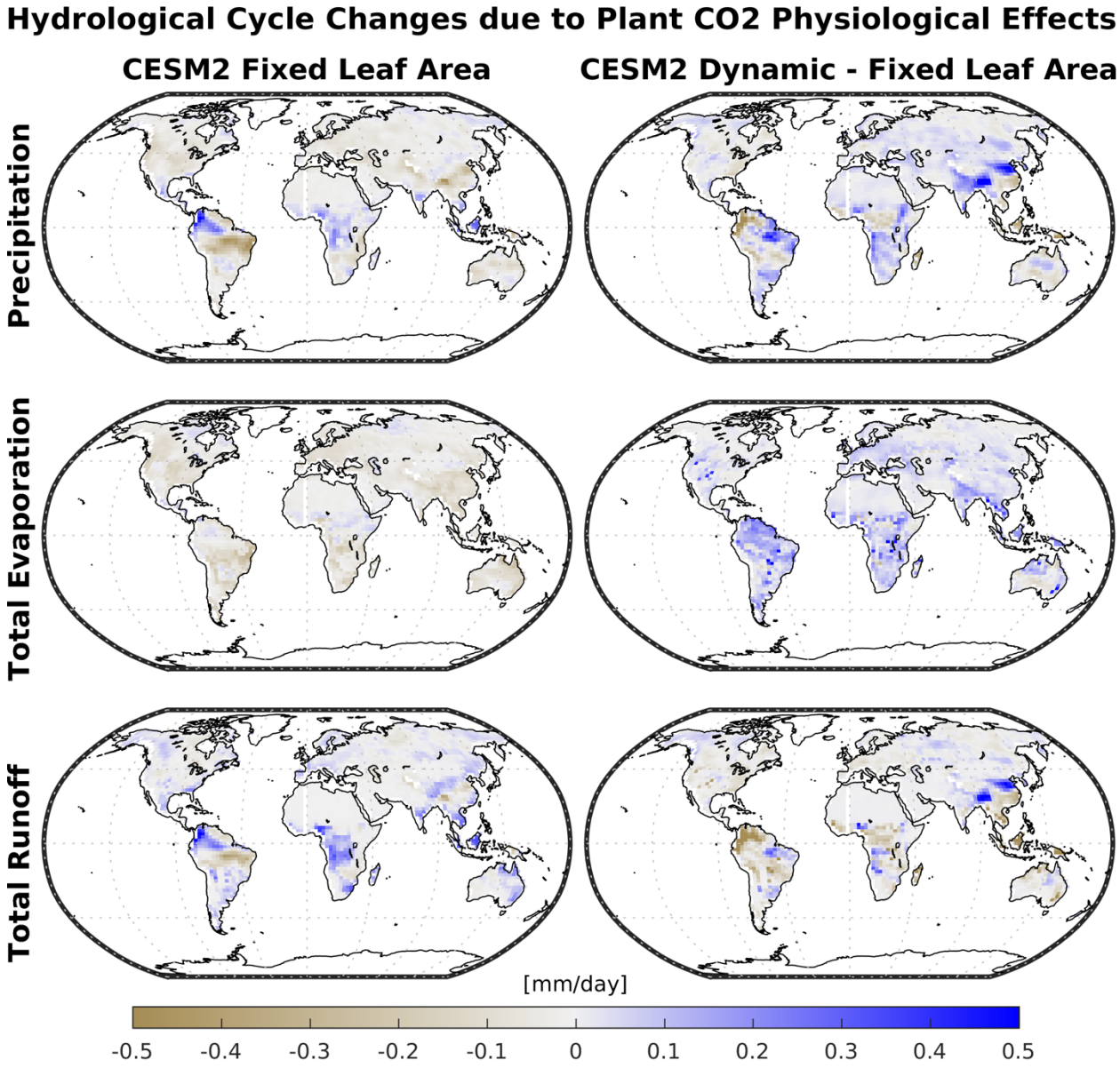

Figure S11. Changes in precipitation, total evaporation, and total runoff between preindustrial CO_2 and 2x preindustrial CO_2 for CESM2 fixed [left column] and dynamic minus fixed [right column] leaf area phys-only runs.

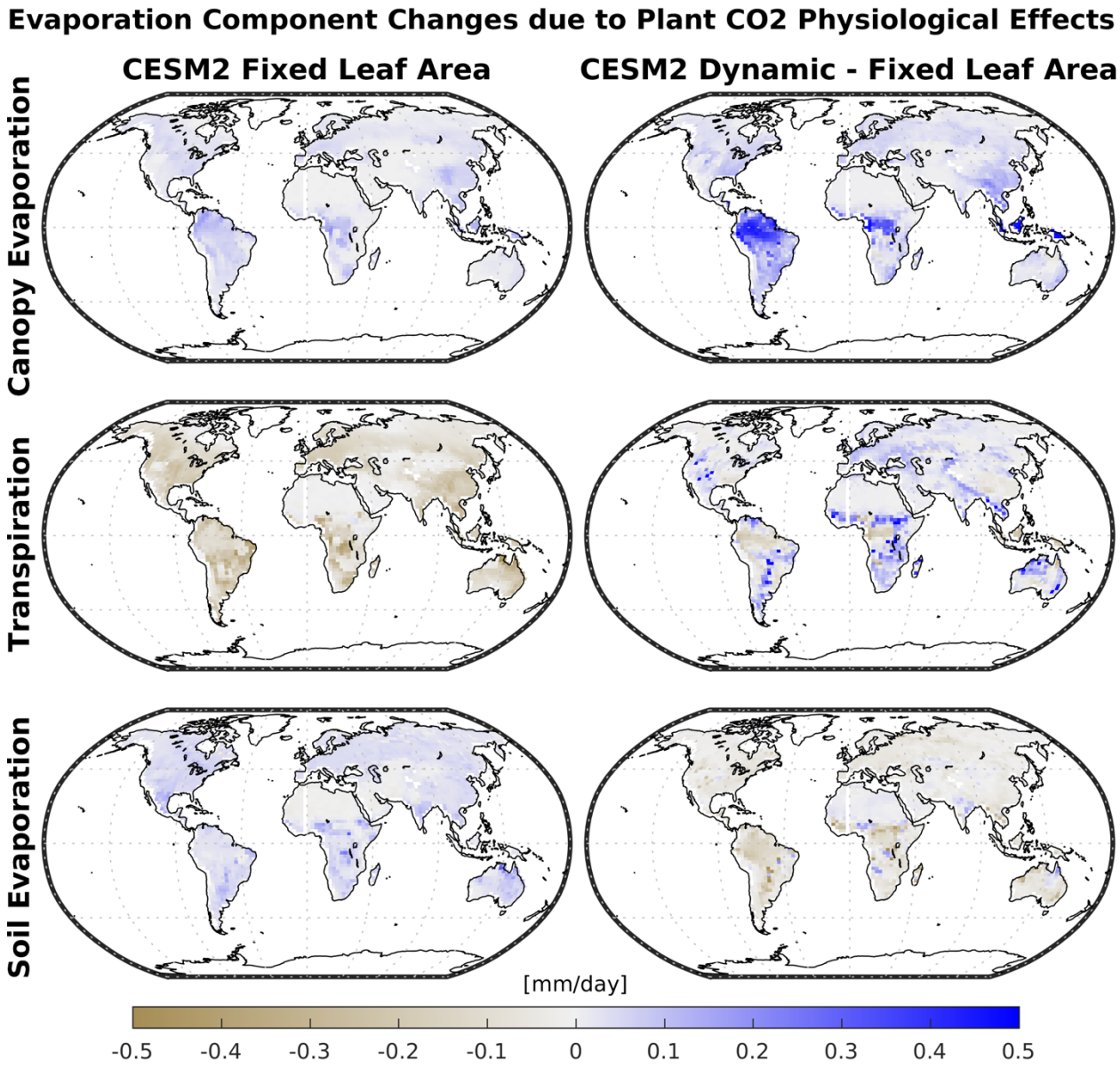

Figure S12. Changes in the components of total evaporation (i.e., canopy evaporation, transpiration, and soil evaporation) between preindustrial CO_2 and 2x preindustrial CO_2 for CESM2 fixed [left column] and dynamic minus fixed [right column] leaf area phys-only runs.

APPENDIX C

RESULTS SECTION 3 SUPPLEMENTAL FIGURES

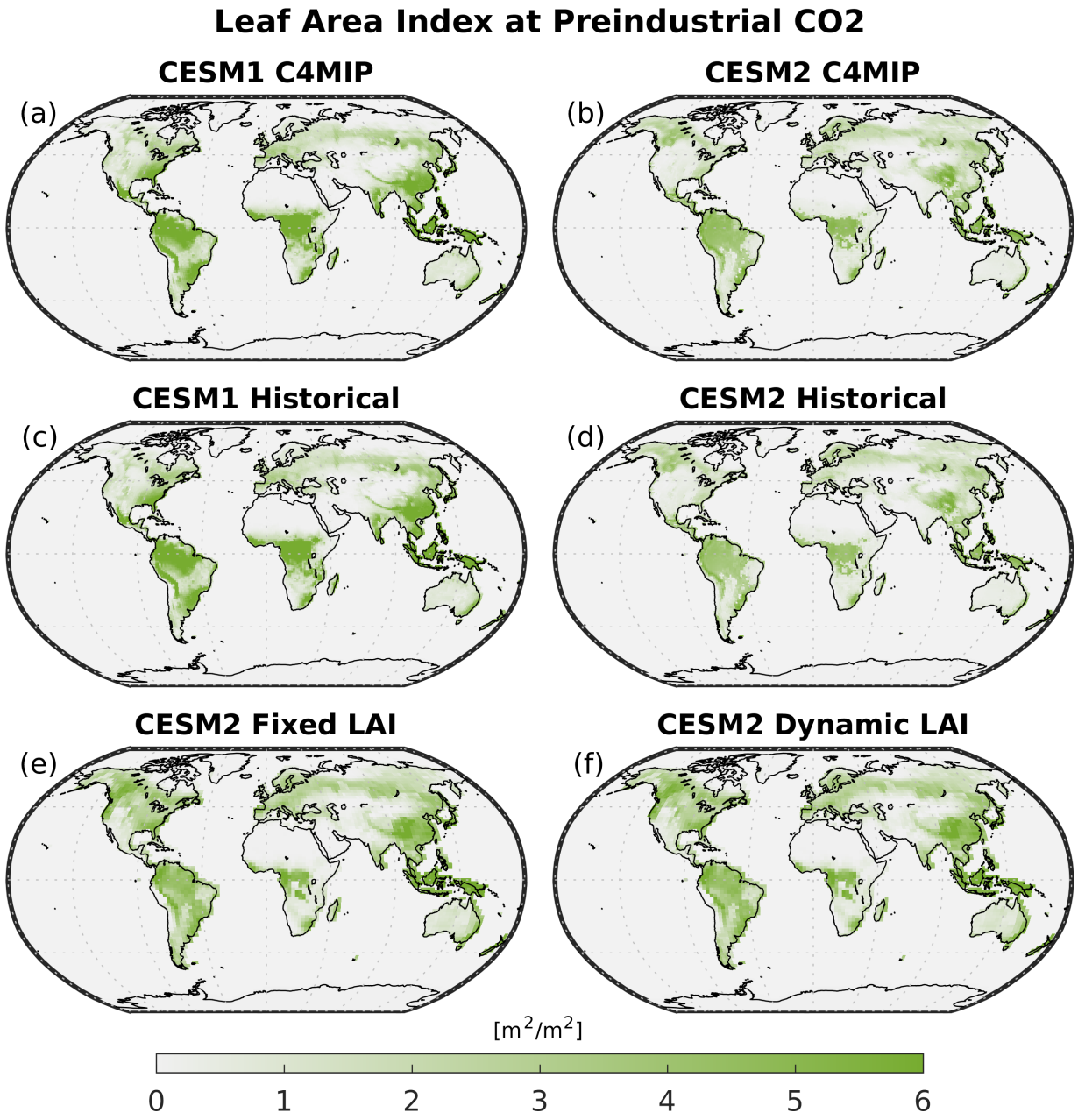

Figure S13. Leaf area at preindustrial CO_2 for (a) CESM1 and (b) CESM2 C4MIP phys-only, (c) CESM1 and (d) CESM2 historical, and (e) CESM2 fixed and (f) dynamic leaf area phys-only simulations.

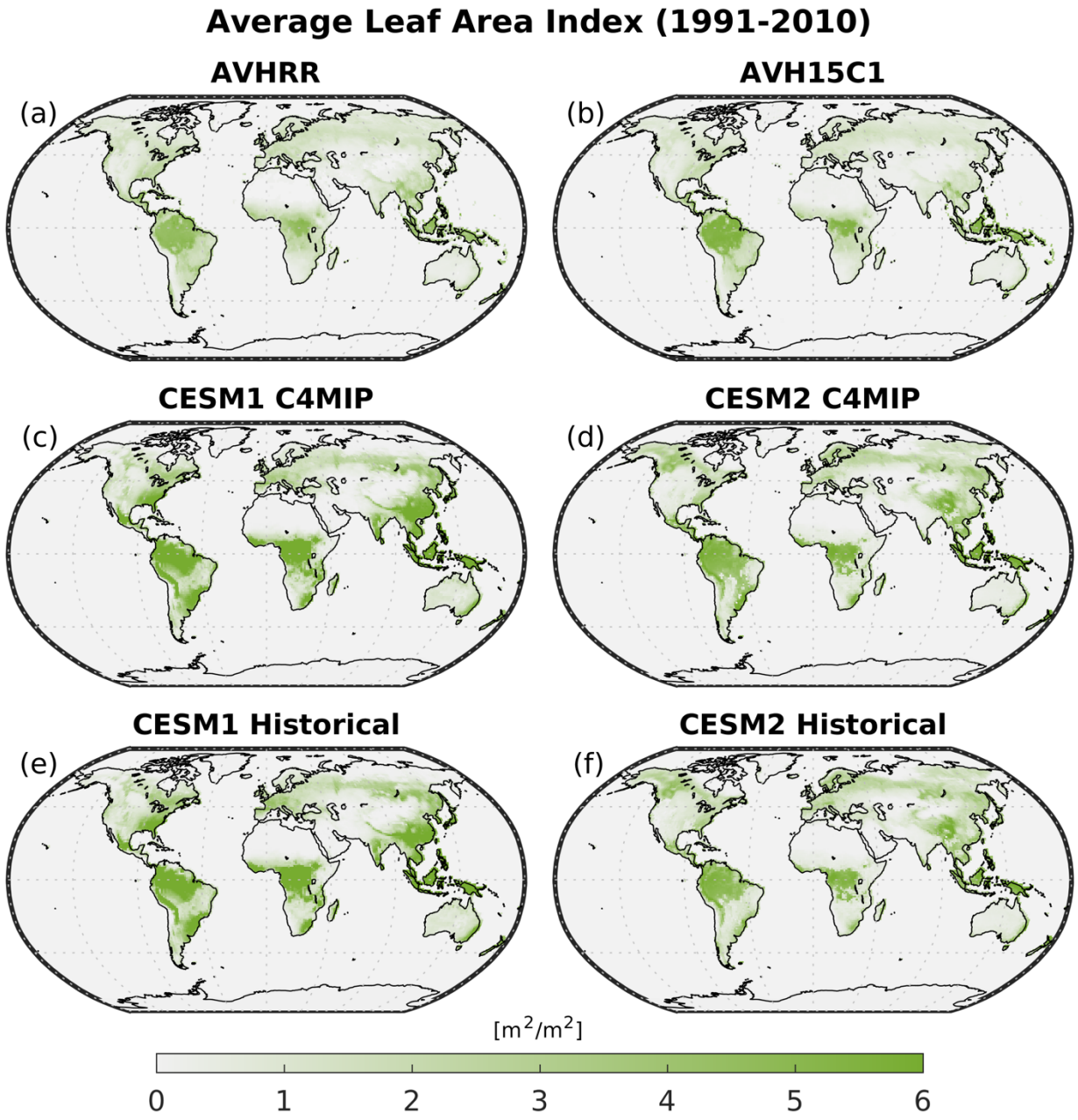

Figure S14. Leaf area index averaged over 1991 to 2010 for (a) AVHRR and (b) AVH15C1 observations, (c) CESM1 and (d) CESM2 C4MIP phys-only experiments, and (e) CESM1 and (f) CESM2 historical simulations.

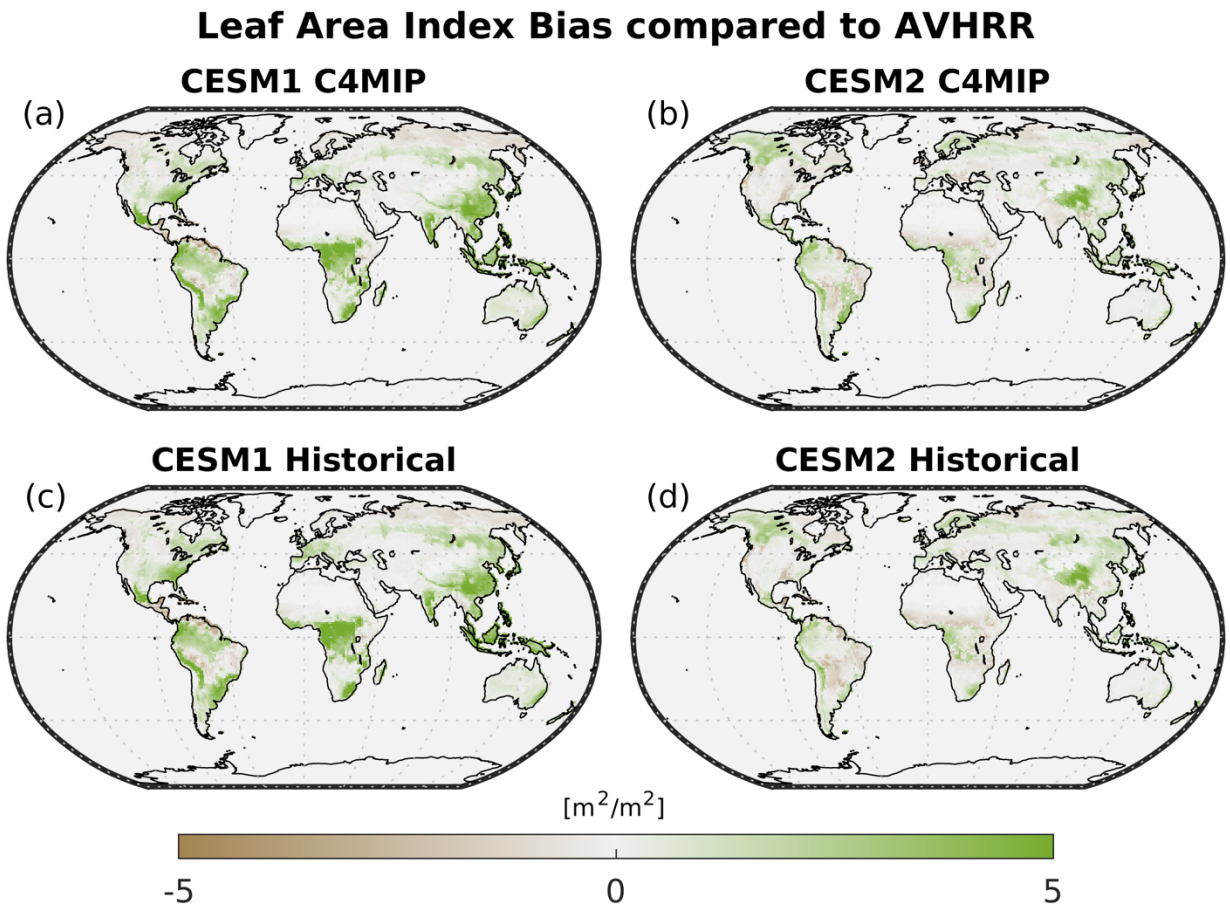

Figure S15. Bias in leaf area index averaged over 1991 to 2010 and calculated as the difference between AVHRR observations and (a) CESM1 and (b) CESM2 C4MIP phys-only experiments, and (c) CESM1 and (d) CESM2 historical simulations.

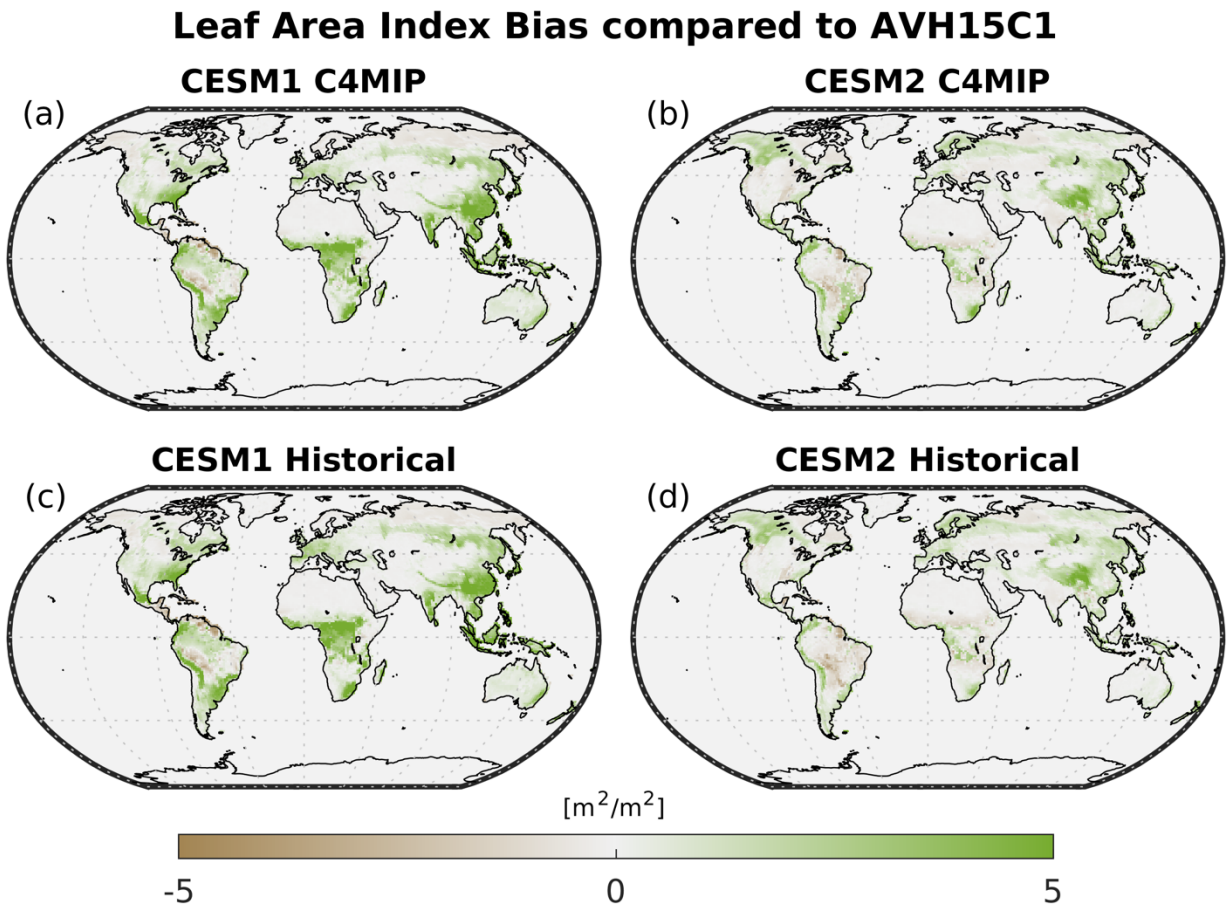

Figure S16. Bias in leaf area index averaged over 1991 to 2010 and calculated as the difference between AVH15C1 observations and (a) CESM1 and (b) CESM2 C4MIP phys-only experiments, and (c) CESM1 and (d) CESM2 historical simulations.

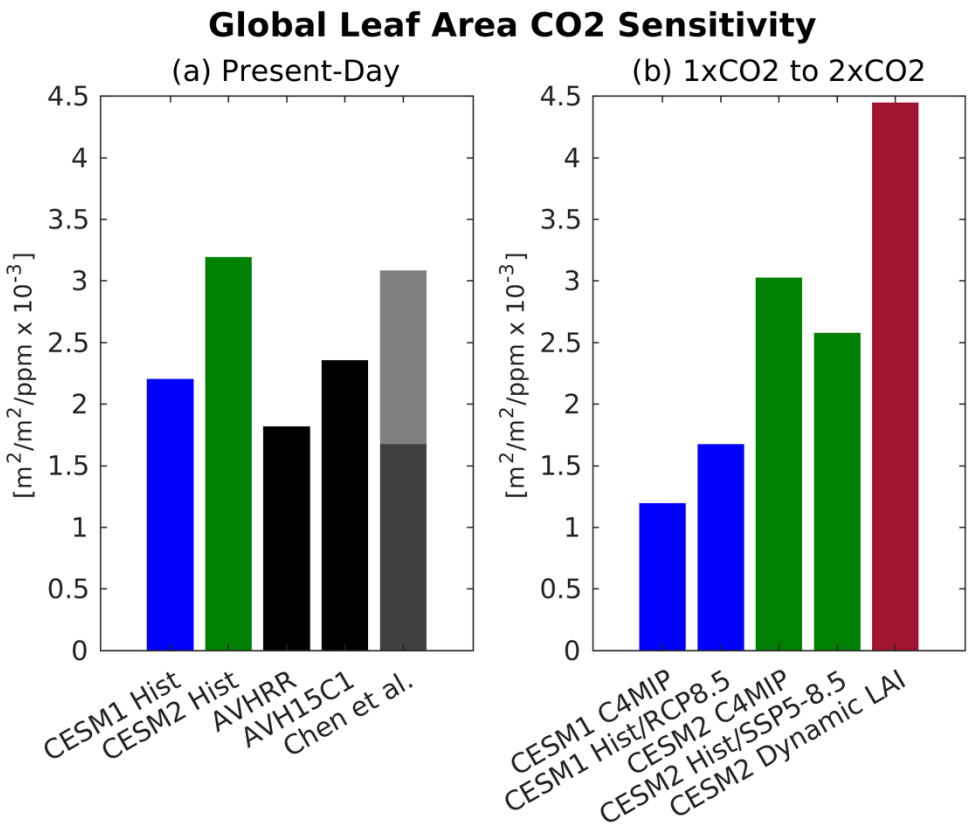

Figure S17. Leaf area sensitivities for the (a) near present-day CO_2 range for CESM1 and CESM2 historical simulations [blue and green bars], AVHRR and AVH15C1 observations [black bars], and Chen et al. (2019) observations [two-tone grey bar], and for (b) preindustrial CO_2 to 2x preindustrial CO_2 for CESM1 C4MIP phys-only and historical extended with RCP8.5 [blue bars], CESM2 C4MIP phys-only and historical extended with SSP5-8.5 [green bars], and CESM2 dynamic leaf area phys-only simulations [red bar]. Two grey colors in Chet et al. bar represent minimum and maximum values in observed LAI sensitivities.